


Immune-modulated adhesive hydrogel for enhancing osteochondral graft adhesion and cartilage repair

Jiaqi Zhou^{a,b,1}, Xiongfa Ji^{a,b,1}, Yu Xue^{c,1}, Wenjie Yang^{a,b},
Guoqing Zhong^{a,b,2,*}, Zhiyang Zhou^{a,b}, Xingmei Chen^c, Zehua Lei^{a,b}, Teliang Lu^d,
Yu Zhang^{a,b,**,2}, Ji Liu^{c,2,***}, Limin Ma^{a,b,e,****,2} 

^a Department of Orthopedics, Guangdong Provincial People's Hospital, Guangdong Academy of Medical Sciences, Southern Medical University, Guangzhou, 510080, China

^b Guang Dong Engineering Technology Research Center of Functional, Repair of Bone Defects and Biomaterials, Guangzhou, 510080, China

^c Department of Mechanical and Energy Engineering, Southern University of Science and Technology, Shenzhen, 518055, China

^d National Engineering Research Center for Healthcare Devices, Guangdong Key Lab of Medical Electronic Instruments and Polymer Material Products, Institute of Biological and Medical Engineering, Guangdong Academy of Sciences, Guangzhou, Guangdong, 510316, China

^e Department of Orthopedics, Ganzhou Hospital of Guangdong Provincial People's Hospital, Ganzhou Municipal Hospital, NO. 49, Dadong Road, Ganzhou, Jiangxi Province, 341000, China

ARTICLE INFO

Keywords:

Hydrogel bioadhesives
Bioadhesion
Injectable
Osteochondral regeneration
Osteochondral autograft transfer system

ABSTRACT

Osteochondral autograft transfer system (OATS) can effectively improve cartilage injuries by obtaining bone-cartilage grafts from healthy sites and implanting them into the defective areas. However, in up to 40 % of patients, the lack of a stable adhesive interface between the osteochondral graft and the normal tissue surface reduces the repair efficiency. In this work, we report an injectable and biocompatible poly (N-hydroxyethyl acrylamide-N-hydroxy succinimide)/Gelatin (PHE-Gel) hydrogel, featuring the instant formation of a tough bio-interface, which allows for robust adhesion with osteochondral grafts. Through physicochemical characterization, we found that a system composed of 10%PHE-Gel possesses superior interfacial toughness and excellent biocompatibility. In vitro, mechanistic studies and RNA-seq analysis had shown that 10%PHE-Gel promotes the expression of cartilage anabolic metabolism genes by upregulating the hypoxia-inducible factor alpha (HIF- α) signaling pathway and downregulating the tumor necrosis factor (TNF) signaling pathway. Dimethyl-ox-allylglycine (DMOG) loaded liposome (DMOG-Lip) promotes the transition of M1 macrophages to M2 macrophages, shifting the microenvironment towards a pro-repair direction. Studies on a rabbit OATS model indicated that DMOG-Lip loaded 10%PHE-Gel (10%PHE-Gel@DMOG-Lip) effectively modulated the immune microenvironment, facilitated the repair of the hyaline cartilage, and inhibited further degeneration of cartilage. This composite hydrogel offers a promising solution for enhancing OATS repair in tissue engineering and has the potential to improve outcomes in cartilage restoration procedures.

Peer review under the responsibility of KeAi Communications Co., Ltd.

* Corresponding author. Department of Orthopedics, Guangdong Provincial People's Hospital, Guangdong Academy of Medical Sciences, Southern Medical University, Guangzhou, 510080, China.

** Corresponding author. Department of Orthopedics, Guangdong Provincial People's Hospital, Guangdong Academy of Medical Sciences, Southern Medical University, Guangzhou, 510080, China.

*** Corresponding author.

**** Corresponding author. Department of Orthopedics, Guangdong Provincial People's Hospital, Guangdong Academy of Medical Sciences, Southern Medical University, Guangzhou, 510080, China.

E-mail addresses: gqzhong@foxmail.com (G. Zhong), luck_2001@126.com (Y. Zhang), liuj9@sustech.edu.cn (J. Liu), malimin7@126.com (L. Ma).

¹ These authors have contributed equally.

² Co-corresponding author

<https://doi.org/10.1016/j.bioactmat.2025.02.035>

Received 7 January 2025; Received in revised form 18 February 2025; Accepted 23 February 2025

2452-199X/© 2025 The Authors. Publishing services by Elsevier B.V. on behalf of KeAi Communications Co. Ltd. This is an open access article under the CC BY-NC-ND license (<http://creativecommons.org/licenses/by-nc-nd/4.0/>).

1. Introduction

Articular cartilage injury with a low capacity for self-repair frequently causes cartilage degeneration and fibrocartilage repair [1], which significantly impacts the patient's quality of life [2]. A review of 31,516 knee arthroscopies by Curl et al. revealed that 63 % of the patients exhibited cartilage injuries [3]. Current therapeutic modalities for articular cartilage injuries include pharmacotherapy, microfracture, autologous chondrocyte transplantation, and arthroplasty [4–6]. Among them, the osteochondral autograft transfer system (OATS), a type of autologous cartilage transplantation, has shown improved clinical results for decades [7]. By obtaining osteochondral plugs from healthy areas and implanting them into the defective areas, OATS achieves hyaline cartilage repair and maintains joint height and shape [8,9]. However, approximately 40 % of patients experience incomplete integration at the border zone [10], suggesting that the interfacial integration of implants with adjacent cartilage remains a challenge in OATS. There exist some difficult-to-fill voids between the implants and the adjacent cartilage, leading to fibrocartilage formation [11]. Subsequently, some patients experience the degeneration of regenerative fibrocartilage, which can lead to plug loosening and degradation, affecting joint function [12]. Therefore, new strategies for filling the void space and promoting cartilage interfacial integration need to be explored.

Hydrogels are materials with high water content [13]. With their capacity to carry cells and several bioactive chemicals, hydrogels with different mechanical properties show promise for tissue regeneration [14,15]. Considering the features of OATS, hydrogels used for filling the void space must have biocompatibility and adhesive properties. It is difficult for traditional hydrogels to support mechanical loads from surrounding plugs and maintain interface stabilization due to their brittle and low-adhesive properties [16,17]. An implant is considered osseointegrated when there is no relative movement between it and the bone it is in direct contact with [18]. Like osseointegration, maintaining the relative stability of the interface is essential for the subsequent cartilage repair process. In this case, bioadhesive hydrogels were reported for noninvasive joint wound closure and cartilage injury repair [19–21]. Moreover, modulation of mechanical properties of the hydrogel could influence the healing process, for example, slower relaxing non-adhesion gels hinder chondrogenesis [22]. Nevertheless, there is currently no adhesive hydrogel that is suitable for the interface of osteochondral transplantation.

Physiologically lacking blood vessels, cartilage, and subchondral bone remain hypoxic [23]. Hypoxia inducible factor- α (HIF- α), the main transcriptional regulator of cellular and developmental response to hypoxia, is essential for chondrocyte homeostasis [24]. Osteoclasts are over-activated in the early stage of osteoarthritis, destroying the joint hypoxic microenvironment and aggravating cartilage degeneration [23]. In the inflammatory environment created by cartilage injury, mesenchymal stem cells undergo aberrant differentiation, causing the subsequent fibrocartilage formation [25]. Therefore, to achieve high-quality cartilage repair, maintaining the hypoxic microenvironment and suppressing the inflammatory response are required. Dimethylallyl Glycine (DMOG), an inhibitor of HIF- α degrading enzymes, stabilizes HIF- α protein expression in chondrocytes and promotes chondrogenic differentiation. Compared to other HIF- α stabilizing compounds such as deferoxamine (DFX) and cobalt chloride (CoCl₂), DMOG induced a stronger chondrogenic transcriptional profile and facilitated selective up-regulation of HIF- α target genes [26]. It was reported that DMOG inhibited the M1 polarization of macrophages and down-regulated the expression of inflammatory factors [27]. At the same time, DMOG promoted the expression of M2 polarization-associated genes, shifting the microenvironment toward a pro-repair direction [28]. Therefore, DMOG is a candidate for regulating the cartilage repair process as a therapeutic agent.

In summary, while significant progress has been made in

understanding the mechanisms of cartilage repair, an effective treatment for articular cartilage injuries remains elusive. The current therapeutic strategies have shown limited success, and there is a critical need for novel approaches that can enhance the integration of grafts with native cartilage and promote the regeneration of hyaline cartilage. In this study, we designed a novel DMOG-loaded adhesive hydrogel wherein the poly (N-hydroxyethyl acrylamide)/gelatin adhesive hydrogel (PHE-Gel) stabilizes the interface and enhances chondrogenic differentiation, while DMOG-loaded liposomes (DMOG-Lip) modulate the immune microenvironment (Scheme 1). We investigated the structural properties, interfacial toughness, and biocompatibility of this hydrogel. Additionally, we assessed cartilage formation and the modulation of the immune microenvironment through in vitro experiments. Finally, we explored the in vivo therapeutic potential of hydrogel for improving hyaline cartilage repair post-OATS surgery.

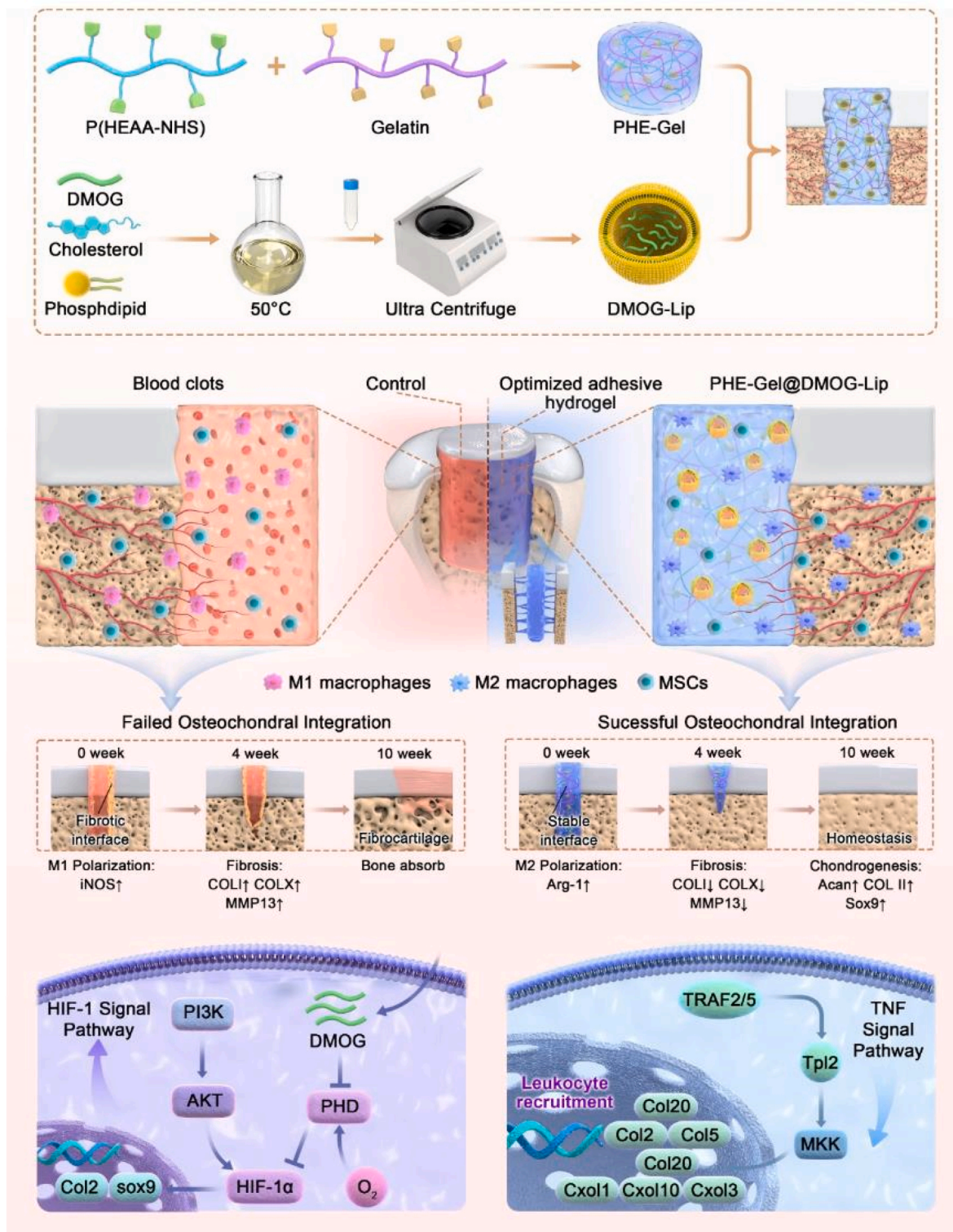
2. Results and discussion

2.1. Preparation and characterization of PHE-gel hydrogel

The formation of the injectable hydrogel adhesive is a result of multiple cross-linking between poly (N-hydroxyethyl acrylamide-N-hydroxy succinimide) [P(HEAA-NHS)] polymer and gelatin, including the chemical cross-linking of NHS to amino groups ($-NH_2$) and hydrogen bond interactions (Fig. 1A). Upon mixing through the syringe, the hydrogel transitions from a liquid to a gel phase within approximately 10 s, with its modulus gradually stabilizing after 500 s, indicating that a stable cross-linking network was formed (Fig. 1B and C). In its liquid phase, the hydrogel is readily injectable onto various tissue contours, establishing a conformal contact with biological substrates. This superior adhesion is attributable to the chemical anchoring effect of NHS, which reacts with amino groups present on the tissue surfaces, and the intertwining of polymer chains contributes to the mechanical dissipation of PHE-Gel hydrogel. It is particularly noteworthy that the hydrogel's adhesion to biological tissues, such as porcine skin, markedly enhances as the content of P(HEAA-NHS) polymer increases from 0 % to 10 % (Fig. 1D and E). This is reflected by a significant increase in interfacial toughness, from 45 to 120 J/m², and a rise in shear strength, from 20 to 45 kPa (Fig. 1F). However, when the P(HEAA-NHS) polymer content is further increased to 20 %, there is a slight decline in adhesive properties. This could be attributed to the higher content of amino groups, which expedites the hydrogel's curing process, potentially precluding the formation of a fully conformal adhesive interface with the tissue. We further added a comparison with commercially available adhesives, showing a breakthrough in adhesion performance. Considering the curing time and adhesive properties, we chose the PHE-Gel hydrogel with 10 % P(HEAA-NHS) and 30 % gelatin (10%PHE-Gel). The adhesive properties of this hydrogel were further substantiated on cartilage, with a shear strength of 40 kPa, affirming its suitability for in vivo cartilage repair applications (Fig. 1G). Moreover, the biopolymers in the PHE-Gel hydrogel are biodegradable by endogenous enzymes (3 mg/mL lysozyme) within a PBS solution within just 14 days (Fig. 1H), ensuring its temporary presence in the body and minimizing any potential long-term implications.

2.2. Biocompatibility of 10%PHE-Gel hydrogel

The cytocompatibility of 10%PHE-Gel was evaluated using Cell Viability/Cytotoxicity tests, Cell Counting Kit-8 (CCK-8) assays, and Hemolysis tests. The 2D in vitro cell culture model revealed minimal cell death at 24 h via Calcein Acetoxymethyl Ester (Calcein-AM)/Propidium Iodide (PI) staining, indicating the non-toxic effects of the hydrogel on cell viability (Fig. S1A). Furthermore, CCK-8 assays demonstrated that the PHE-Gel hydrogel exhibited no significant cytotoxicity at 24, 48, and 72 h compared to controls, thereby not impeding cell proliferation (Fig. S1B). Hemolysis tests further confirmed the non-toxic nature of the



Scheme 1. The design and fabrication process of DMOG liposome-loaded P(HEAA-NHS)/Gelatin (PHE-Gel@DMOG-Lip) hydrogel adhesive for the integration of osteochondral grafting.

gel, as there were no significant differences in hemolysis rates compared to the control (Fig. S1C). Collectively, these results affirm the satisfactory cytocompatibility of 10%PHE-Gel hydrogel.

Research into the regulation of mesenchymal stem cell (MSC) differentiation by factors like cell shape, mechanical forces, extracellular matrix, and geometric structures has provided key insights for advancing stem cell-based cartilage tissue regeneration and engineering

[29]. MSCs undergo extensive contraction and establish N-cadherin-mediated cell-cell adhesion, thereby initiating cartilage differentiation [30]. Detailed cytoskeletal staining reveals that in low-adhesive hydrogels such as the PHE-Gel hydrogel with 5 % P(HEAA-NHS) and 30 % gelatin (5%PHE-Gel), MSCs predominantly exhibit a spindle-shaped morphology. However, as the adhesive of the hydrogel increases, there are significant cytoskeletal adjustments, causing the cells to adopt

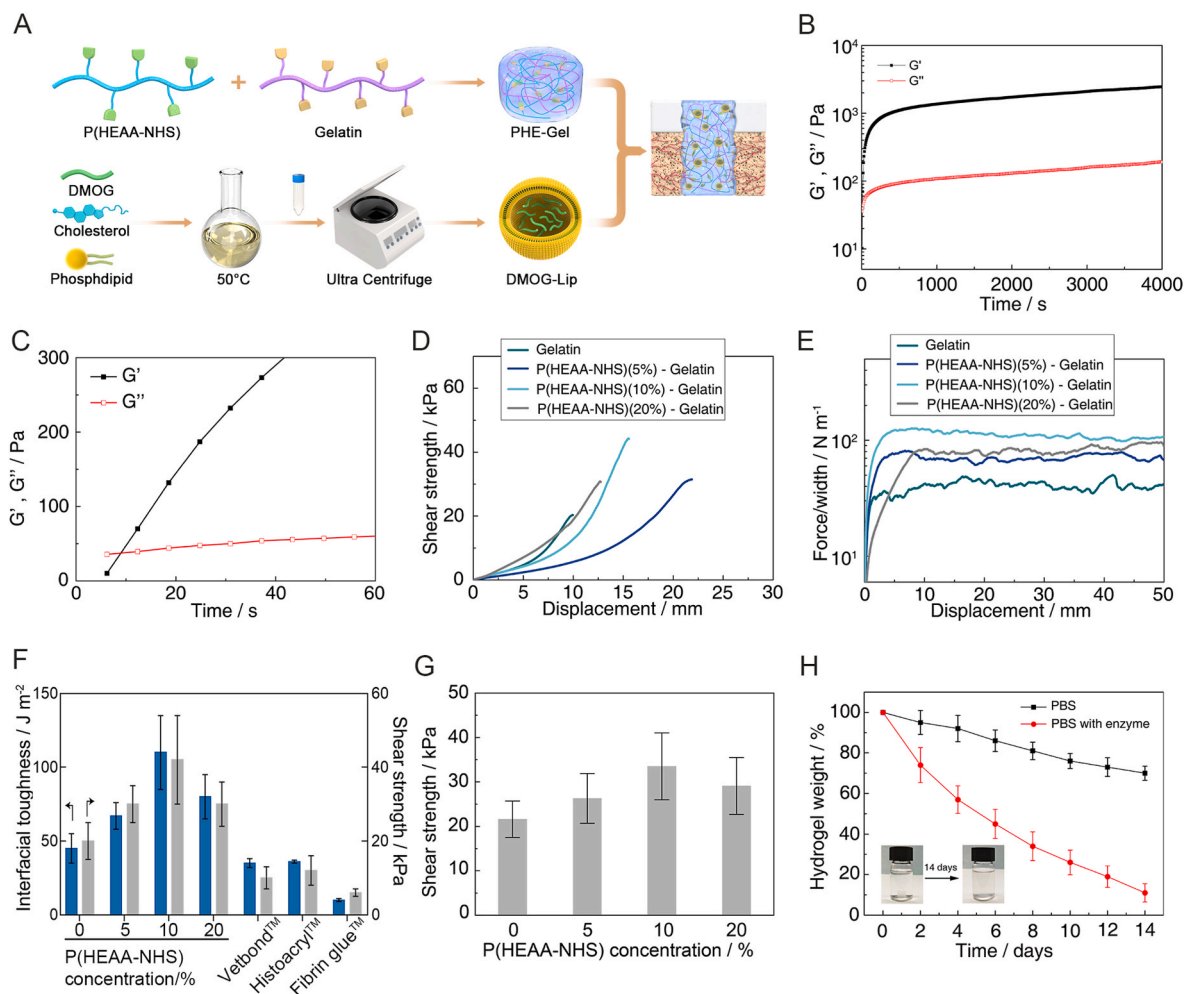


Fig. 1. Preparation and characterization of injectable PHE-Gel hydrogel adhesive. (A) Schematic of injectable PHE-Gel and PHE-Gel@DMOG-Lip hydrogel formation process. Injectable PHE-Gel hydrogel adhesives were prepared by mixing the P(HEAA-NHS) (0 %, 5 %, 10 %, and 20 %, w/v) and gelatin (30 %, w/v) evenly using a syringe. DMOG-loaded liposomes were thoroughly blended with gelatin and then combined with P(HEAA-NHS) to generate PHE-Gel@DMOG-Lip hydrogel. (B) Dynamic time sweep rheological analysis to evaluate gelation kinetics of PHE-Gel hydrogel. (C) The crossing point of G' and G'' is considered as the gelation time. (D) The representative lap shear test curves with shear stress plotted against displacement. (E) The representative peeling curves with peeling force per width plotted against displacement. (F) Summary of adhesive performance of commercially available adhesives and injectable PHE-Gel hydrogel, which is composed of various fractions of P(HEAA-NHS). (G) PHE-Gel hydrogel-cartilage interface strength measured by shear tests. (H) *In vitro* enzyme-catalyzed degradation of the hydrogel samples. Hydrogel samples soaked in pure PBS buffer were tested as a control, featuring a slight weight change. Data are presented as mean \pm S.D., $n = 5$.

a more rounded shape. This transition in cell morphology is particularly pronounced following the addition of DMOG-Lip, which is known to modulate cellular responses and potentially enhance hypoxic conditions that favor chondrogenesis (Fig. S2). These observations suggest that the PHE-Gel hydrogel has a profound impact on the physical environment of the stem cells, potentially influencing their differentiation pathway. The changes in adhesive and the presence of specific biochemical agents like DMOG-Lip demonstrate that the physical and chemical properties of the hydrogel can be finely tuned to direct MSC fate.

To evaluate the biocompatibility and immune modulation of implanted hydrogels, a static subcutaneous implantation model was used for preliminary studies. Briefly, 10%PHE-Gel and DMOG-Lip loaded 10%PHE-Gel (10%PHE-Gel@DMOG-Lip) hydrogels were subcutaneously implanted into rabbits and harvested at 2, 4, and 8 weeks to evaluate their fibrous capsule formation and immune responses. From a macroscopic view, it was observed that both 10%PHE-Gel and 10%PHE-Gel@DMOG-Lip groups gradually degraded by week 8 with little vascular proliferation, indicating the hydrogels' degradability and weak inflammatory properties (Figs. S3A and S3B).

Histological staining with H&E showed that both 10%PHE-Gel and 10%PHE-Gel@DMOG-Lip induced collagen decomposition around the

hydrogel, with minimal infiltration of inflammatory cells (Fig. S4). Masson's staining was further used to illustrate the distribution of formed collagen and inflammatory cells. Macroscopically, the results showed that both 10%PHE-Gel and 10%PHE-Gel@DMOG-Lip groups had inflammatory cell infiltration at week 2, but a higher density of collagen encapsulation was observed at weeks 4 and 8 in the 10%PHE-Gel group (Fig. S3C). Tissue sections also revealed the degradation of the hydrogel. By week 4, remnants of the hydrogel (light blue in Masson staining) were observed in both 10%PHE-Gel and 10%PHE-Gel@DMOG-Lip, but the hydrogel volume was larger in the 10%PHE-Gel@DMOG-Lip group, possibly due to its weak inflammatory properties reducing the infiltration and phagocytosis by inflammatory cells.

2.3. Chondrogenesis and mechanism of PHE-gel hydrogel

By adjusting the content of P(HEAA-NHS), the adhesive properties and pore distribution of the hydrogel can be modified, as shown in Fig. 1G and Fig. S5. Scanning electron microscopy (SEM) showed that the 10%PHE-Gel samples contained noticeable pores (Fig. S5A), which facilitated the encapsulation of liposomes and preserved their native morphology. Detailed release curves showed that 10%PHE-Gel hydrogel

could effectively achieve sustained release of DMOG (Fig. S5E). For chondrogenesis, we used PHE-Gel with different content of P(HEAA-NHS), and gelatin alone was used as a control to assess the effect of hydrogels on the chondrogenic differentiation of mouse embryonic fibroblasts (C3H/10T1/2, C3H10) without chondrogenic induction. qRT-PCR results showed that, within a 3-day intervention period, 10%PHE-Gel significantly increased the expression of cartilage-related genes Aggrecan (Acan), SRY-Box Transcription Factor 9 (Sox9), and Collagen II (Col2a1), whereas the PHE-Gel hydrogel with 20 % P(HEAA-NHS) and 30 % gelatin (20%PHE-Gel) and 5%PHE-Gel did not show significant effects (Fig. 2A–C). The results of Western blot analysis indicated that while the 10%PHE-Gel group did not significantly enhance Collagen II (Col2) expression, it markedly elevated Sox9 levels (Fig. 2I). This discrepancy may be attributed to the limited duration of the intervention, suggesting that longer exposure times may be necessary to observe effects on chondrogenesis. As the intervention period extended to seven days, the 10%PHE-Gel group maintained a high level of chondrogenic induction capability (Fig. 2D–F and 2J). This phenomenon was further validated through Immunofluorescence staining (Fig. 2G and H), indicating that the adhesive of PHE-Gel plays a significant role in chondrogenic differentiation. Consequently, 10%PHE-Gel was selected as the suitable adhesive hydrogel for osteochondral transplantation due to its high adhesive properties and effective cartilage regeneration.

To assess the chondrogenic potential of 10%PHE-Gel@DMOG-Lip, we performed a stem cell intervention study with induction media. qRT-PCR analysis revealed that the expression of chondrogenic markers Acan, Sox9, and Col2a1 was significantly upregulated exclusively in the 10%PHE-Gel@DMOG-Lip group at both 7- and 14-days post-intervention (Figs. S6A–F). Immunofluorescence staining of Sox9 also demonstrated that the composite component exhibited a superior induction effect on chondrogenic differentiation (Figs. S6G and S6H). In addition, the results of western blotting showed that the expression of Sox9 and Col2 was significantly up-regulated in the 10%PHE-Gel@DMOG-Lip group (Fig. S6H). Alcian blue staining also showed that the 10%PHE-Gel@DMOG-Lip group had more mucopolysaccharide extracellular matrix (Fig. S6J). These findings suggest that the synergistic application of DMOG-Lip and the PHE-Gel demonstrates superior chondrogenic induction capabilities compared to the individual components or the control group. We further evaluated the effects of DMOG-Lip and hydrogel on cartilage degeneration markers COL3 and MMP13. Although DMOG-Lip and hydrogel alone had little effect on cartilage anabolic indexes ACAN and COL2, they could significantly reduce cartilage degeneration and maintain cartilage phenotype (Fig. S7D).

To explore the underlying mechanism, RNA-seq analysis employed time-series transcriptome sequencing to analyze the changes in gene expression of stem cells under different viscosities of PHE-Gel intervention. The bioinformatics analysis of RNA-seq results in the Gelatin control, 5%PHE-Gel group, 10%PHE-Gel, 20%PHE-Gel, DMOG-Lip, and 10%PHE-Gel@DMOG-Lip was performed using mfuzz package (Fig. 3A).

In the 7-day group, we identified 9750 differentially expressed genes which clustered into four distinct groups reflecting varied expression patterns. KEGG enrichment analysis on these clusters, with a focus on cartilage-related pathways, revealed the following: Cluster 1's expression decreased with rising hydrogel's adhesion and was further reduced by DMOG, implicating Extracellular Matrix (ECM) receptor interaction, TNF, and Peroxisome Proliferators-activated Receptor (PPAR) pathways. Cluster 2's expression rose with rising hydrogel's adhesion and DMOG addition, involving HIF-1, Hippo, Adenosine 5'-monophosphate activated protein kinase (AMPK), Focal adhesion, PI3K-Akt, Wnt, and TGF-beta pathways. Cluster 4's expression increased with rising hydrogel's adhesion but decreased with solo DMOG, yet combining DMOG with 10%PHE-Gel elevated expression, highlighting PI3K-Akt, ECM-receptor interaction, and Hippo pathways (Figs. S7A–C).

In the 14-day group, 8159 differentially expressed genes were identified, forming four distinct clusters that each depicted unique

expression patterns. The genes in Cluster 1 exhibited increased expression levels with rising hydrogel adhesion and were enriched in the “Biosynthesis of cofactors” and “Purine metabolism” pathways. The expression levels of genes in Cluster 2 decreased with increasing hydrogel adhesion, and their expression further declined upon DMOG addition. These genes were primarily enriched in the KEGG pathways of “ECM-receptor interaction,” “Focal adhesion,” and “TNF signaling pathway”, indicating that 10%PHE-Gel and DMOG-Lip promote osteochondral repair by affecting cell adhesive behavior and reducing inflammatory responses. Cluster 3 contained genes upregulated upon the addition of DMOG-Lip, which were mainly enriched in the “Biosynthesis of amino acids”, “HIF-1 signaling pathway”, and “PI3K/Akt pathway”, suggesting that DMOG-Lip promotes the repair process by activating the HIF pathway and regulating metabolism (Fig. 3B–D). We further validated the RNA-Seq results using WB and found that DMOG-Lip significantly upregulated HIF expression and downregulated TNF expression (Fig. S7D). Supplementary cell migration experiments suggested that DMOG-Lip effectively promoted the migration of stem cells and recruited more stem cells during the early repair process (Fig. S7E). This effect would facilitate tissue integration and initiate the cartilage repair process.

2.4. 10%PHE-Gel@DMOG-lip modulates local immune microenvironment for tissue regeneration

The natural healing of osteochondral defects is often accompanied by an immune storm, which can easily lead to the formation of fibrous cartilage instead of hyaline cartilage. Therefore, regulating the local inflammatory microenvironment in the early stages of repair is crucial for creating a regenerative microenvironment. Macrophages are considered classical immune cells, and their polarization state reflects the state of the local immune microenvironment. Inducible Nitric Oxide Synthase (iNOS) can be used as a marker for the degree of inflammation, while Arginase-1 (Arg-1) serves as a marker for the extent of regeneration. Under in vitro conditions where lipopolysaccharide (LPS) induces the M1 polarization of bone marrow-derived macrophages (BMDMs), interventions were performed using PBS control group (Con), 10%PHE-Gel, DMOG-Lip, and 10%PHE-Gel@DMOG-Lip. qRT-PCR results showed that both 10%PHE-Gel and DMOG-Lip could downregulate iNOS expression and upregulate Arg-1 (Fig. 4D and E). This phenomenon was further validated through Immunofluorescence staining (Fig. 4A–C). Similarly, the M1 macrophage polarization markers interleukin-1 β (IL-1 β) and TNF- α exhibited a comparable downregulation effect, while the M2 macrophage polarization marker mannose receptor (CD206) was upregulated in the 10%PHE-Gel and DMOG-Lip groups (Fig. S8).

IF staining was further used to evaluate the immune microenvironment in vivo (Fig. 4F and G). Results showed that in the early stages of subcutaneous implantation, 10%PHE-Gel@DMOG-Lip compared to the 10%PHE-Gel group exhibited significant suppression of the inflammatory marker iNOS expression and promoted the expression of the anti-inflammatory marker Arg-1. By week 4, iNOS expression was significantly increased in the 10%PHE-Gel group, likely due to a foreign body inflammatory response to the hydrogel, while DMOG-Lip significantly reduced this marker. Similarly, Arg-1 expression was significantly higher in the 10%PHE-Gel@DMOG-Lip group compared to the 10% PHE-Gel group, suggesting that DMOG-Lip promotes polarization towards M2 macrophages. By week 8, there were no significant differences in the fluorescence intensities of iNOS and Arg-1 between the two groups, and the levels were comparable to those at week 2, proving that 10%PHE-Gel is fully degradable and that the addition of DMOG-Lip can reduce the inflammatory response and fibrogenesis.

2.5. The 10%PHE-Gel@DMOG-lip hydrogel stabilizes the interface and maintains cartilage homeostasis in the rabbit OATS model

Based on the results from subcutaneous implantation, we used the

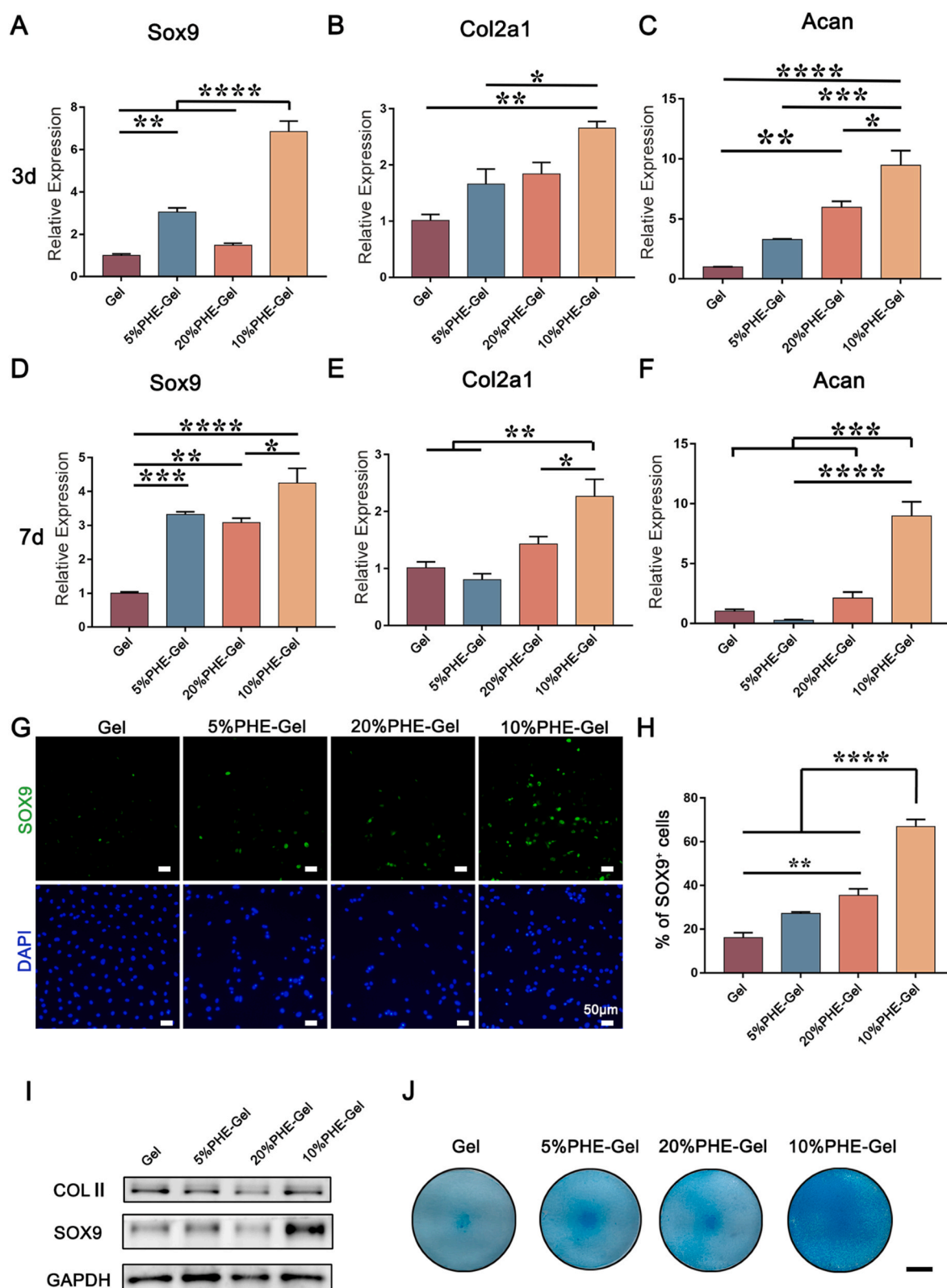


Fig. 2. Chondrogenic induction of different adhesive PHE-Gel hydrogel. Gene expression analysis at day 3. (A) Sox9 mRNA relative expression levels. (B) Col2a1 mRNA relative expression levels. (C) ACAN mRNA relative expression levels. Gene expression analysis on day 7. (D) Sox9 mRNA relative expression levels. (E) Col2a1 mRNA relative expression levels. (F) ACAN mRNA relative expression levels. (G) Immunofluorescence staining on day 7. SOX9 staining (upper row). DAPI nuclear staining (lower row). (H) Percentage of SOX9-positive cells at day 7. (I) Western blot result on day 3. (J) Alcian blue staining on day 7. Scale bar, 4 mm. Data are presented as mean \pm S.D., $n = 3$. Statistical significance is indicated by asterisks, with * $p < 0.05$, ** $p < 0.01$, *** $p < 0.001$, and **** $p < 0.0001$.

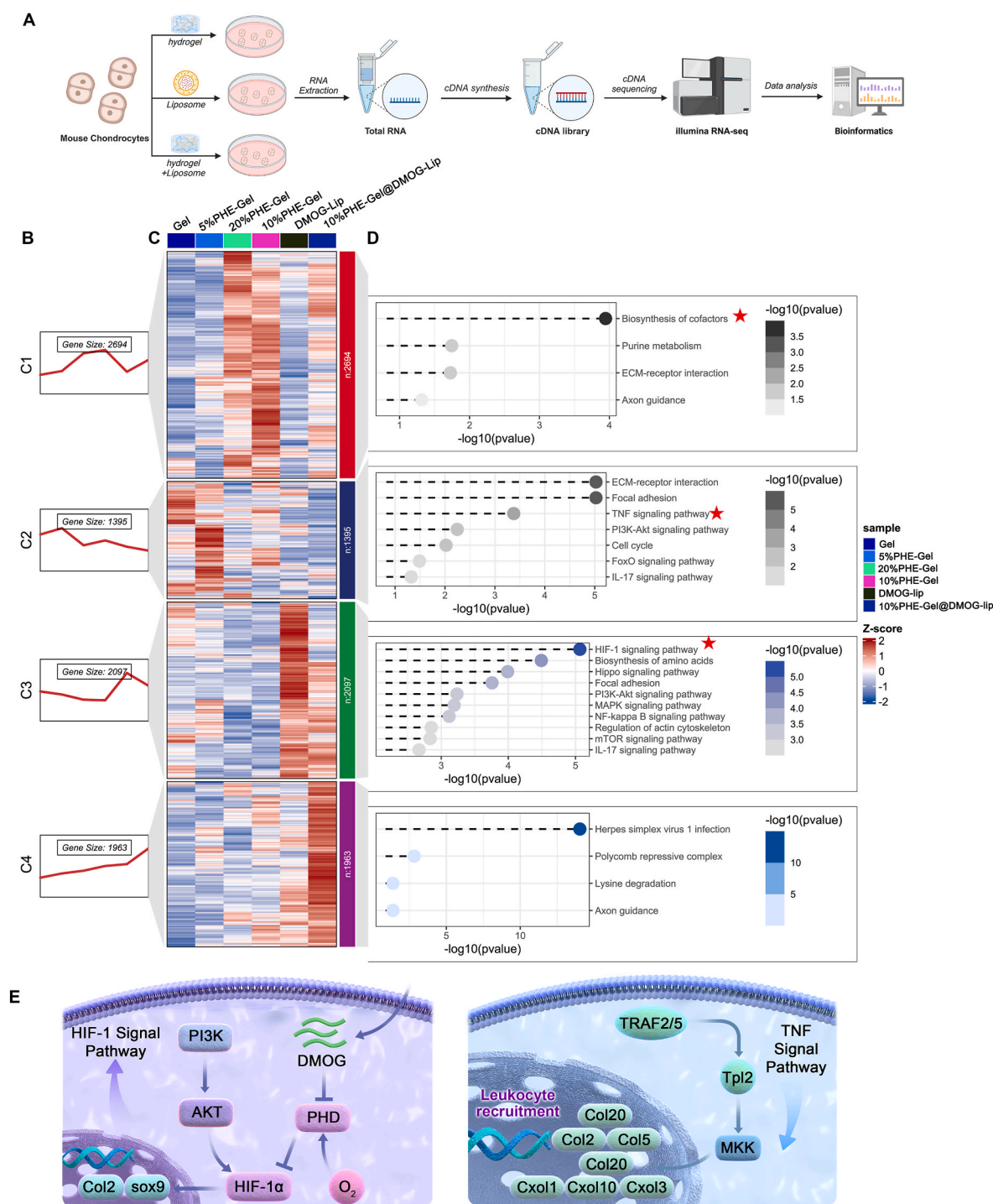


Fig. 3. RNA-seq analysis of mesenchymal stem cells (MSCs) treated with different adhesive PHE-Gel hydrogel. (A) Flowchart of RNA-seq and bioinformatics analysis. Mfuzz soft clustering analysis of 8159 differentially expressed genes (DEGs) identified in the 14-day treatment group. (B) The line chart displays the expression dynamics of genes in each of the four clusters across different treatment groups: Gel, 5%PHE-Gel, 10%PHE-Gel, 20%PHE-Gel, DMOG-Lip, and 10%PHE-Gel@DMOG-Lip. Each line represents the dynamics of the gene cluster, and the color indicates cluster membership. (C) Heatmap visualization of the DEGs, showing the expression levels of genes in each cluster across the treatment groups. The color intensity represents the normalized expression value, with red indicating a higher expression and blue indicating a lower expression. Treatment groups are shown on the x-axis, and DEGs are arranged on the y-axis. (D) KEGG pathway enrichment analysis for each gene cluster. The bar plot displays the top enriched KEGG pathways for genes in each cluster, with the x-axis representing the enrichment score or p-value and the y-axis listing the KEGG pathway terms. The color of the bars indicates the corresponding cluster, consistent with the colors used in the line chart and heatmap. (E) Mechanism schematic of the underlying mechanism 10%PHE-Gel@DMOG-Lip for MSCs.

New Zealand white rabbit OATS model to evaluate the promoting effect of adhesive hydrogels on the repair of the bone cartilage interface. Full-thickness, 4-mm-diameter cylindrical articular cartilage defects were created at the middle of the femoral condyles of the knee joint using a

trephine drill. The resulting osteochondral tissue blocks were re-implanted into the defect site to assess the repair effect of bone cartilage transplantation (Fig. 5A). The simple transplantation without hydrogel group served as the control, where a weak adhesive was

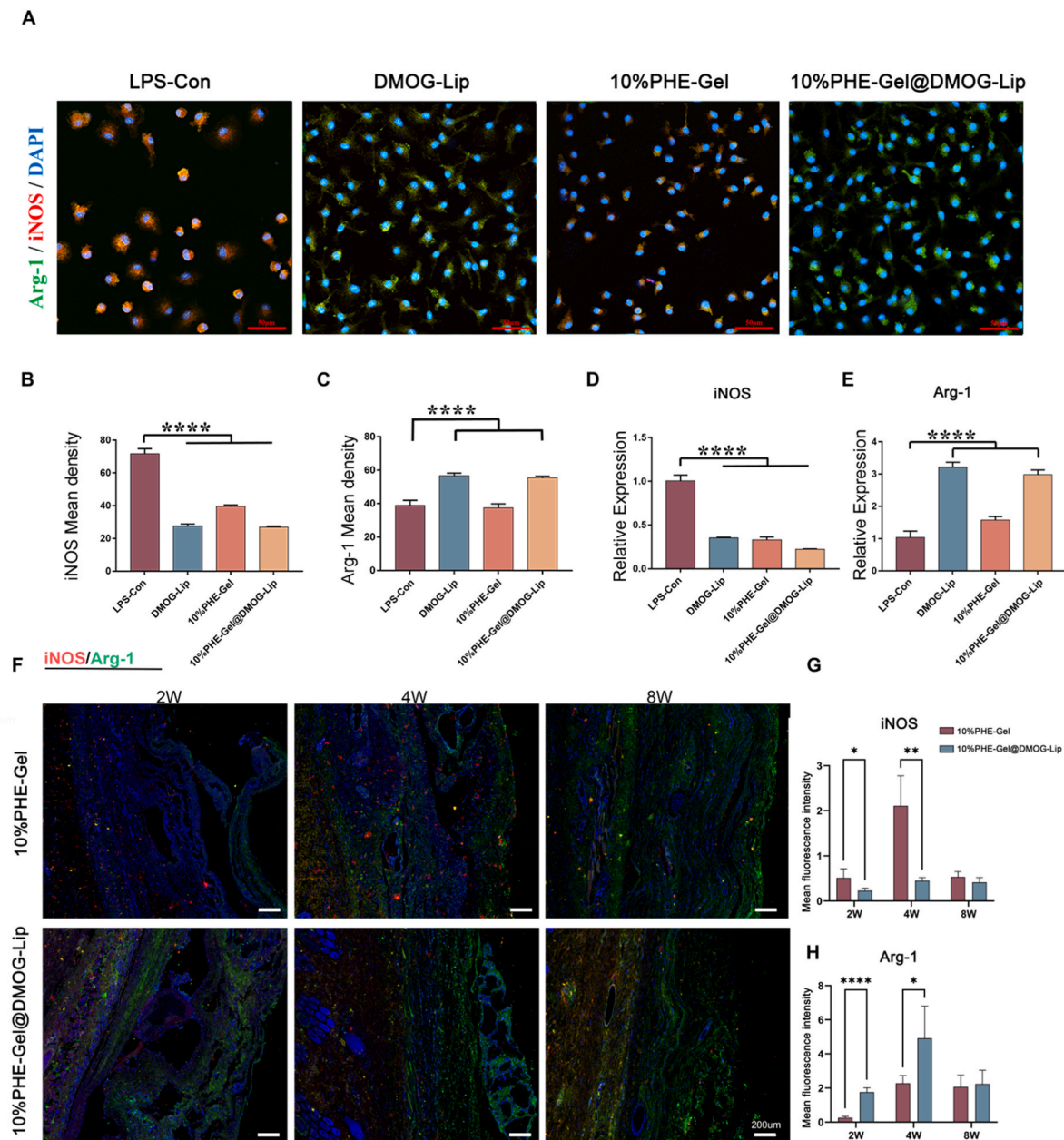


Fig. 4. Evaluation of immune modulatory properties of 10%PHE-Gel@DMOG-Lip hydrogel. (A) Immunofluorescence images showing iNOS (red) and Arg-1 (green) expression in different treatment conditions: LPS (LPS-Con), DMOG-Lip, 10%PHE-Gel, and 10%PHE-Gel@DMOG-Lip. Cell nuclei are stained blue with DAPI. Scale bar, 10 μ m. (B–C) Quantification of the mean density of iNOS and Arg-1 expression in BMDMs with different treatments. (D–E) Relative gene expression of iNOS and Arg-1 in BMDMs treated with different intervention groups for 24 h under LPS-induced inflammatory stimulation, indicating immune response modulation. (F) Immunofluorescence staining for iNOS (red) and Arg-1 (green) in subcutaneous implantations of 10%PHE-Gel and 10%PHE-Gel@DMOG-Lip at 2, 4, and 8 weeks, showing differential expression patterns. Scale bar, 200 μ m. (G–H) Quantification of mean fluorescent intensity of iNOS and Arg-1 expression in the 10%PHE-Gel and 10%PHE-Gel@DMOG-Lip groups at 2, 4, and 8 weeks, illustrating changes in inflammatory and healing responses over time. Data are presented as mean \pm S.D., $n = 3$ (in vitro), $n = 6$ (in vivo). Statistical significance is indicated by asterisks, with * $p < 0.05$, ** $p < 0.01$, *** $p < 0.001$, and **** $p < 0.0001$.

formed between the transplanted tissue and the original bone cartilage by a blood clot formed by bone marrow fluid. The addition of adhesive hydrogels at the interface to promote integration was considered the experimental group, with the hydrogel base system used in this study being a highly adhesive hydrogel with superior chondrogenic properties selected through in vitro screening. Similar to the in vitro experiments, the 10%PHE-Gel formed rapidly and integrated with the surrounding tissue. These results suggest that the high-adhesive hydrogels are quick-gelling, mechanically strong, highly adhesive, and thus can firmly stabilize the transplanted tissue and the damaged bone cartilage interface.

To further evaluate the potential of 10%PHE-Gel@DMOG-Lip in

cartilage repair and regeneration, osteochondral-implanted 36 rabbits were divided into three groups: PBS control, 10%PHE-Gel, and 10%PHE-Gel@DMOG-Lip. Specimens were obtained at 4- and 10-week post-surgery for analysis. Gross observation revealed that at 4 weeks, there was a clear gap between the graft and the surrounding cartilage in the control group. In the 10%PHE-Gel and 10%PHE-Gel@DMOG-Lip groups, the boundary between the graft and the surrounding cartilage was smoother, but the position of the graft could still be distinguished, indicating that tissue integration was not yet complete. At 10 weeks, the graft position in the control group showed significant absorption and collapse, while in the 10%PHE-Gel group, the boundary between the

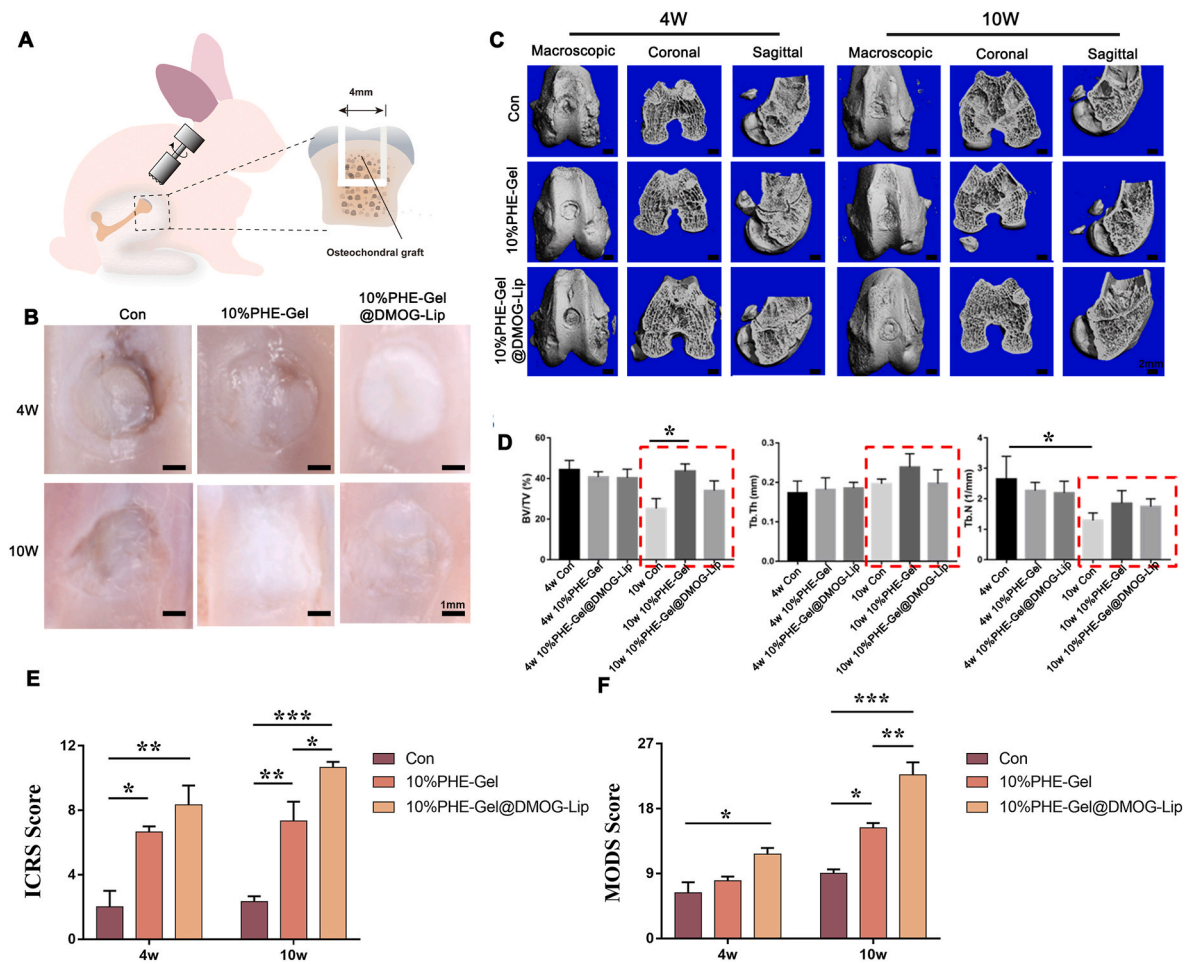


Fig. 5. In vivo application of 10%PHE-Gel@DMOG-Lip and micro-CT Analysis. (A) Schematic representation of the rabbit osteochondral autograft transfer (OATS) surgery. (B) Macroscopic view of the femoral trochlea surface in the control, 10%PHE-Gel, and 10%PHE-Gel@DMOG-lip groups at 4- and 10-weeks post-OATS surgery. Scale bar, 1 mm. (C) Three-dimensional (3D) reconstruction of micro-CT scans in the control, 10%PHE-Gel, and 10%PHE-Gel@DMOG-lip groups at 4- and 10-weeks post-OATS surgery. Representative macroscopic, coronal, and sagittal views are shown. Scale bar, 2 mm. (D) Quantitative analysis of subchondral bone parameters, including bone volume fraction (BV/TV), trabecular thickness (Tb.Th), and trabecular number (Tb.N), in the control, 10%PHE-Gel, and 10%PHE-Gel@DMOG-lip groups at 4 and 10 weeks post-OATS surgery. (E–F) Quantification of International Cartilage Repair Society (ICRS) and modified O'Driscoll histologic scores (MODS). Data are presented as mean ± S.D., $n = 6$. Statistical significance is indicated by asterisks, with * $p < 0.05$, ** $p < 0.01$, *** $p < 0.001$.

graft and the surrounding cartilage had basically disappeared, but the position of the graft could still be distinguished, indicating that tissue integration was still incomplete. In contrast, the 10%PHE-Gel@DMOG-Lip group exhibited near-perfect integration, with the graft and surrounding cartilage being almost indistinguishable (Fig. 5B).

We further used micro-CT analysis of the obtained bone specimens to assess the integration of subchondral bone. The three-dimensional reconstruction results showed that at 4 weeks, the graft position exhibited varying degrees of collapse, while at 10 weeks, recovery was observed, and the joint surface tended to be smooth, indicating that subchondral bone underwent continuous remodeling during tissue integration (Fig. 5C and Fig. S9). Quantitative analysis revealed that in the early stage of bone remodeling (4 weeks), there were no significant differences in bone volume fraction (BV/TV), trabecular thickness (Tb.Th), and trabecular number (Tb.N) among the groups, suggesting that the transplanted subchondral bone had not yet undergone absorption. In the late stage of bone remodeling (10 weeks), the control group showed a significant decrease in BV/TV and Tb.N, indicating severe absorption of the transplanted subchondral bone and osteoporosis. The BV/TV in the 10%PHE-Gel and 10%PHE-Gel@DMOG-Lip groups was equivalent to that of the 4-week samples, suggesting that bone absorption had not occurred. The Tb.Th in the 10%PHE-Gel group showed an increasing trend, while it decreased in the 10%PHE-Gel@DMOG-Lip group,

possibly because 10%PHE-Gel stabilized the interface between the graft and the surrounding bone, favoring bone retain and regeneration, while DMOG-Lip inhibited chondrocyte hypertrophy and mineralization. The lack of time-dependent changes in Tb.N in the 10%PHE-Gel and 10%PHE-Gel@DMOG-Lip groups also confirmed that trabecular bone did not decrease in these two groups, suggesting that 10%PHE-Gel can reduce the occurrence of osteoporosis during osteochondral transplantation (Fig. 5D). We further conducted quantitative analyses of the International Cartilage Repair Society (ICRS) and modified O'Driscoll histologic scores (MODS) on the collected specimens. The results indicated that the repair effect of the DMOG-Lip group was comparable to that of the 10%PHE-Gel group in the short term (4w); however, in the long term (10w), the continuous action of DMOG rendered the DMOG-Lip group significantly superior to the 10%PHE-Gel group (Fig. 5E and F).

As shown in Fig. 6A, in conventional OATS, the interface between the osteochondral graft and defect is typically filled with blood clots, which can ultimately result in cartilage and subchondral bone degeneration. The use of 10%PHE-Gel helps to maintain interfacial stability and promote cartilage repair, although it may lead to eventual cartilage hypertrophy. Furthermore, the continuous release of DMOG has been shown to effectively inhibit cartilage degeneration and maintain cartilage homeostasis. Safranin O staining was performed to evaluate short-

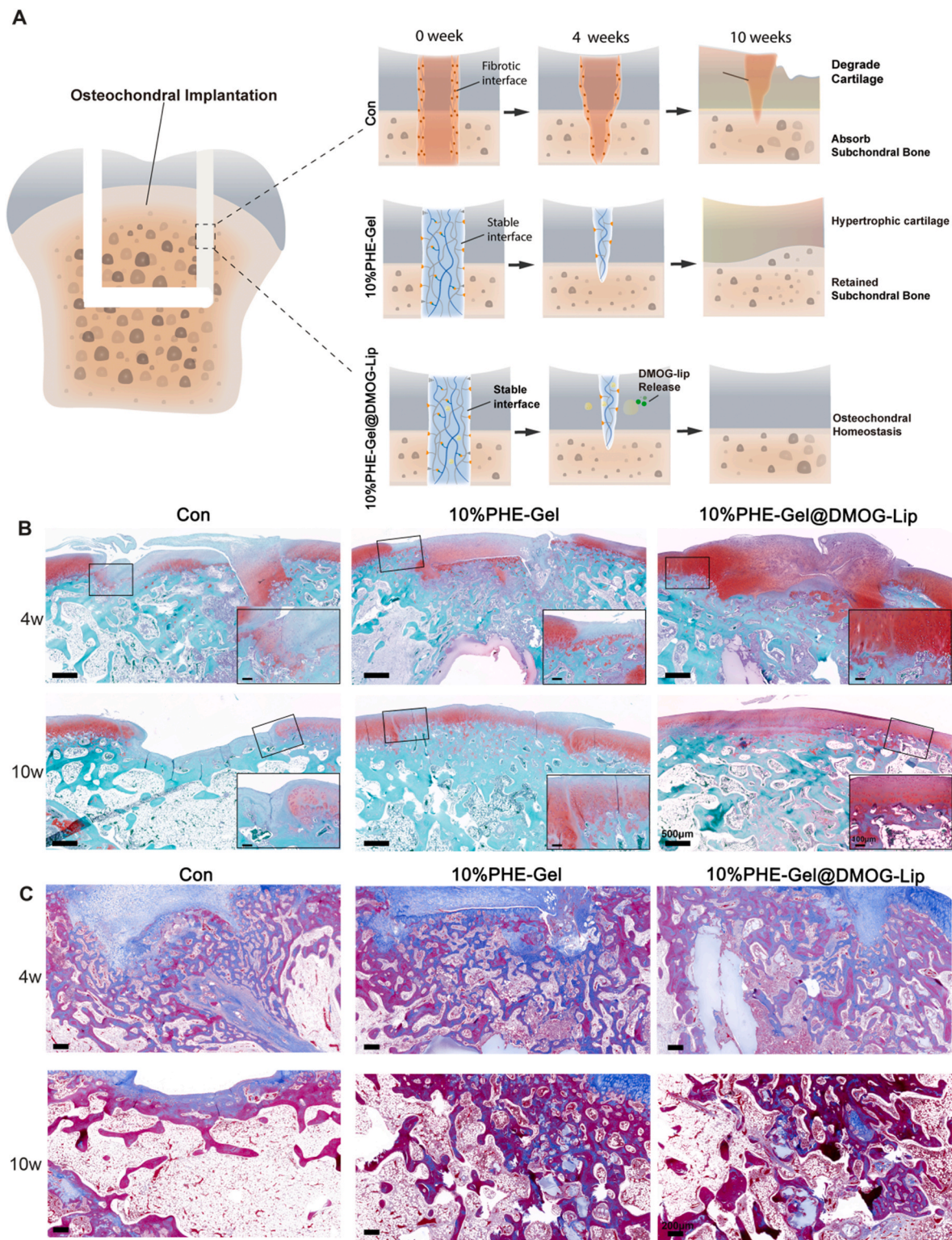


Fig. 6. Osteochondral histological staining of 10%PHE-Gel@DMOG-Lip adhesion in a rabbit OATS model. (A) Schematic representation of the in situ osteochondral healing process in the control, 10%PHE-Gel, and 10%PHE-Gel@DMOG-Lip groups. (B) Safranin-O (S-O) staining of knee cartilage in the control, 10%PHE-Gel, and 10%PHE-Gel@DMOG-Lip groups at 4 and 10 weeks. Scale bar = 500 μ m. For partial enlarged detail, Scale bar = 100 μ m. (C) Masson's trichrome staining of subchondral bone in the control, 10%PHE-Gel, and 10%PHE-Gel@DMOG-Lip groups at 4 and 10 weeks. Scale bar = 200 μ m. $n = 6$.

term cartilage retention and long-term cartilage degradation. At 4 weeks, the control group exhibited matrix degeneration of the transplanted osteochondral graft, with fibrous tissue filling the interface, resulting in an uneven repair. The 10%PHE-Gel group showed mild degeneration, with fibrous tissue filling the interface. However,

compared to the control group, the repair interface was smooth, and the integration of osteochondral tissue was improved. Notably, the 10%PHE-Gel@DMOG-Lip group retained a large amount of cartilage matrix, and the tissue filling the interface was rich in cartilage proteoglycans, indicating the superior cartilage-promoting properties of the drug-

loaded hydrogel. Remarkably, at 8 weeks, the transplanted osteochondral graft in the control group underwent significant degeneration and formed a fibrous-filled depressed area, representing a failure of repair. In the 10%PHE-Gel group, the transplanted cartilage became thinner, but the interface underwent satisfactory cartilage integration, which was also rich in cartilage proteoglycans. Interestingly, the osteochondral graft in the 10%PHE-Gel@DMOG-Lip group retained a thickness like the surrounding native cartilage, and the interface achieved cartilage and bone integration (Fig. 6B). Considering that no adhesive was used in the clinical operation of OATS, fibrin glue was not used as a control in the animal experiment. Even so, with the fibrinogen control group in Yin et al.'s study [31], the same repair effects were observed as in the control group in our experiment. These results demonstrate that the 10% PHE-Gel@DMOG-Lip composite hydrogel is suitable as an adhesive for osteochondral transplantation.

Masson's Trichrome staining is used to evaluate the effectiveness of subchondral bone regeneration and the maintenance of bone homeostasis. The results show that at 4 weeks, the control group's implantation site is surrounded by fibrotic tissue. In the 10%PHE-Gel group, some adhesive hydrogel is visible around the implant, with a small amount of new bone formation connected to the original bone. The structure of the transplanted subchondral bone is stable, with no evidence of bone resorption or damage. The 10%PHE-Gel@DMOG-Lip group is similar to the 10%PHE-Gel group, also showing undegraded hydrogel and newly formed bone. Additionally, there is a deposition of translucent cartilage-like tissue between the cartilage and subchondral bone, suggesting that 10%PHE-Gel@DMOG-Lip promotes cartilage regeneration. By 10-week, significant bone resorption is observed in the subchondral bone of the control group, affecting both the original and transplanted bone. In contrast, both the 10%PHE-Gel and 10%PHE-Gel@DMOG-Lip groups exhibit better maintenance of subchondral bone homeostasis. The hydrogel surrounds the newly formed bone and shows significant degradation, further validating the biocompatibility and degradability of the hydrogel (Fig. 6C). Therefore, the 10%PHE-Gel adhesive hydrogel demonstrates superior performance in maintaining the stability of transplanted subchondral bone and promoting bone integration, with the addition of DMOG-Lip potentially enhancing the integration of cartilage and subchondral bone.

Immunofluorescence staining (IF) was employed to detect the polarization of macrophages at the integration interface at short-term samples (4w). The results showed that the M1 macrophage polarization marker iNOS was highly expressed in the control group, while the addition of 10%PHE-Gel significantly reduced iNOS expression. This phenomenon was more pronounced in the 10%PHE-Gel@DMOG-Lip group, suggesting that 10%PHE-Gel@DMOG-Lip can alleviate inflammation during the repair process, which is consistent with the *in vitro* results (Fig. S10). On the other hand, we evaluated the expression of Arg-1, a marker of macrophages involved in promoting repair at the integration interface. The results demonstrated low expression of Arg-1 in the control group, while 10%PHE-Gel adhesion significantly increased Arg-1 expression, and the addition of DMOG-Lip further enriched Arg-1-positive cells. These findings indicate that 10%PHE-Gel@DMOG-Lip, as an interfacial adhesive for osteochondral grafts, can improve the inflammatory microenvironment and promote osteochondral repair and integration.

We further evaluated the fibrosis and degeneration of regenerated tissues at the integration interface for long-term samples (10w) using immunohistochemistry. The results of Collagen I (COLI), an important marker of fibrosis, showed abundant positive expression in the regenerated cartilage of the control group. Fortunately, COLI expression was significantly reduced in the 10%PHE-Gel group, and the addition of DMOG-Lip further enhanced this effect. The hypertrophic cartilage-related marker Collagen X (COLX) exhibited a similar phenomenon, suggesting that the regenerated cartilage in the control group was mainly fibrocartilage prone to degeneration, while 10%PHE-Gel tended to promote a hyaline cartilage phenotype. Notably, the tissue

degradation-related marker Matrix Metalloproteinase 13 (MMP13) was highly expressed in the control group, indicating active degeneration of the regenerated tissue. In contrast, 10%PHE-Gel reduced MMP13 expression in the regenerated region, and the addition of DMOG-Lip further enhanced this effect, suggesting that the matrix degradation activity of the regenerated cartilage tissue was at a lower level in 10% PHE-Gel@DMOG-Lip group (Fig. 7). In addition, at the last detection point, HE staining was used to evaluate the impact of hydrogel degradation on major organs of the whole body. The results indicated that no significant damage was observed in any of the major organs (Fig. S11), thereby demonstrating that 10%PHE-Gel and 10%PHE-Gel@DMOG-Lip hydrogel also possess excellent biosafety *in vivo*. Overall, the immunohistochemistry results demonstrate that 10%PHE-Gel@DMOG-Lip can promote the generation of stable hyaline cartilage with long-term stability at the integration interface.

3. Conclusion

In this study, we developed a 10%PHE-Gel@DMOG-Lip adhesive to address the challenges associated with the osteochondral autograft transfer system (OATS) in cartilage repair. The optimized 10%PHE-Gel formulation exhibited superior bioadhesion performance, enabling robust integration with osteochondral grafts and sustainable release of DMOG-Lip to ameliorate the hypoxic microenvironment. Our *in vitro* and *in vivo* studies demonstrated that 10%PHE-Gel@DMOG-Lip facilitated macrophage M2 polarization and promoted chondrogenic differentiation of MSCs. RNA-seq analysis provided valuable insights into the molecular mechanisms underlying hydrogel's ability to promote chondrogenesis. The efficacy of 10%PHE-Gel@DMOG-Lip was further validated in a rabbit OATS model, where it successfully healed the interface of cartilage defects, modulated the immune microenvironment, facilitated the repair of the hyaline cartilage, and inhibited further degeneration of cartilage. By addressing the challenges of interfacial integration, void filling, and the hypoxic microenvironment, such adhesive hydrogels were capable of promoting chondrogenesis and immunomodulatory effects, positioning it as a promising candidate to augment OATS repair and enhance outcomes in cartilage restoration procedures. With further development and clinical validation, such hydrogel bioadhesives have the potential to transform the treatment of cartilage defects and improve the quality of life for patients suffering from cartilage injuries.

4. Materials and methods

4.1. Materials

Soya phospholipids, cholesterol, surfactant, dimethyloxalylglycine (DMOG), N-Hydroxyethyl acrylamide, acrylic acid N-hydroxy succinimide ester, 2,2'-Azobis(2-methyl propionitrile), diethyl ether, DSPE-PEG2000, chloroform, TritonX-100, Bovine Serum Albumin (BSA), Collagenase II, ITS+, L-Ascorbic Acid 2-Phosphate Sesquimagnesium Salt Hydrate, proline, dexamethasone, enhanced chemiluminescence reagents, lipopolysaccharides from *E. coli* (LPS), 4',6-diamidino-2-phenylindole (DAPI) and Safranin O/Fast green staining solution were bought from Sigma-Aldrich. Dimethyl Sulfoxide (DMSO), Cell Counting Kit-8 assays, were provided by MedChemExpress. PBS, Fetal bovine serum (FBS), penicillin-streptomycin (P/S), trypsin, Dulbecco's Modified Eagle Medium (DMEM), Dulbecco's Modified Eagle Medium/Nutrient Mixture F-12 (DMEM/F12), Roswell Park Memorial Institute 1640 (RPMI-1640), Minimum Essential Medium Alpha (MEM-alpha) and sodium pyruvate were obtained from Gibco. A nucleic acid purification kit was procured from Omega. TransScript All-in-One First-Strand cDNA Synthesis SuperMix for qPCR was purchased from TransGen. Red blood cell lysate, Calcein-AM/PI Cell Viability/Cytotoxicity Assay Kit, 4 % Paraformaldehyde (PFA) fixative, and TRITC-Phalloidin were provided by Biosharp. 0.9 % saline solution, RIPA Lysis Buffer, protease

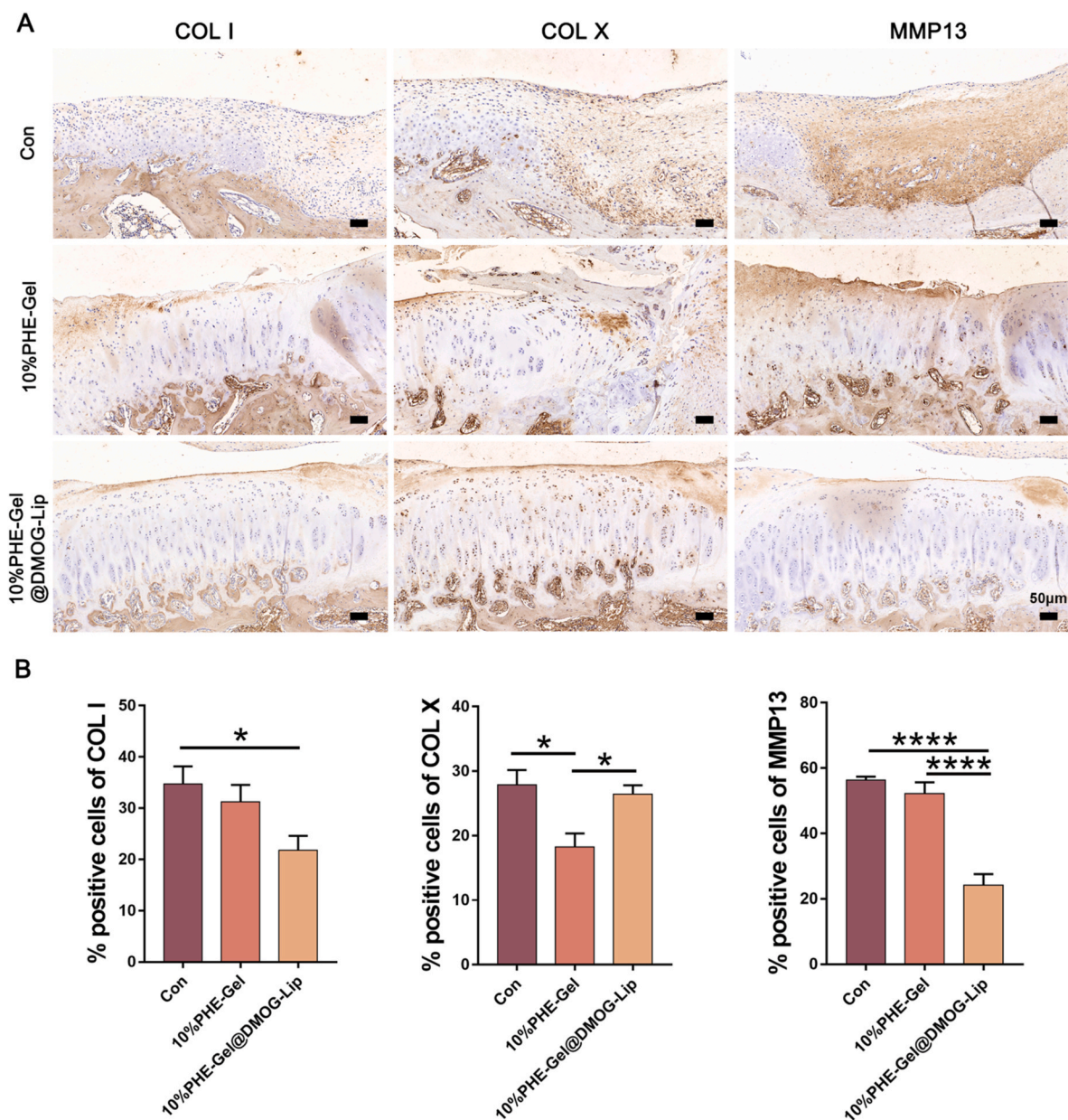


Fig. 7. Immunohistochemistry (IHC) analysis of 10%PHE-Gel@DMOG-Lip adhesion in a rabbit OATS model. (A) Representative IHC images of COLI, COLX, and MMP13 staining in the control, 10%PHE-Gel, and 10%PHE-Gel@DMOG-lip groups at 10 weeks, to evaluate the homogenesis of regenerative cartilage. Scale bar = 50 μm. (B) Quantification of positive cells proportion of COLI, COLX, and MMP13 in the control, 10%PHE-Gel, and 10%PHE-Gel@DMOG-lip groups. Data are presented as mean ± S.D., $n = 6$. Statistical significance is indicated by asterisks, with * $p < 0.05$, **** $p < 0.0001$.

inhibitor cocktail, Phenylmethanesulfonyl fluoride (PMSF), and 5X loading buffer were bought from Beyotime. PVDF membrane was procured from Merck Millipore. Trizol reagent was obtained from Thermo Fisher. Transforming growth factor- $\beta 1$ (TGF- $\beta 1$), macrophage-stimulating factor (M-CSF), interleukin-4 (IL-4), and interleukin-13 (IL-13) were bought from Peprotech. As for the primary antibodies, anti-SOX9 (ab185966) and anti-iNOS (ab49999) were obtained from Abcam, anti-MMP13 (PA5-119271) was bought from Thermo Fisher, anti-iNOS (bs-2072R) was provided by Bioss, and anti-Col I (14695-1-AP), anti-Col X (26984-1-AP), anti-COLII (28459-1-AP) and anti-Arg-1 (16001-1-AP, 66129-1-Ig) were provided by proteintech. As for the secondary antibody, Goat anti-rabbit IgG-Alexa Fluor 488 (ab150077), Goat anti-rabbit IgG-Alexa Fluor 647 (ab150079), Goat anti-mouse IgG-Alexa Fluor 488 (ab150113), Goat Anti-Rabbit IgG H&L (HRP) (ab6721), and Goat anti-mouse IgG-Alexa Fluor 647 (ab150115) were bought from Abcam, Alcian Blue Staining Kit (pH = 2.5) and Masson's

Trichrome Stain Kit were bought from Solarbio.

Adult male C57bl/6 mice (6- to 8-week-old), and New Zealand white rabbits (weighing about 2.5 kg) were provided by Guangdong Medical Laboratory Animal Center. The experimental design was approved by the Animal Ethics and Experiment Committee of Guangdong Provincial People's Hospital (Reference No. KY-D-2021-402-01). Efforts were made to minimize the number of animals and their suffering throughout the whole project.

4.2. Synthesis of the P(HEAA-NHS) copolymers

Briefly, 4.5 g of N-Hydroxyethyl acrylamide (HEAA) and 0.5 g of acrylic acid *N*-hydroxy succinimide ester (AA-NHS ester) were dissolved in dry and degassed DMSO, together with 0.5 wt% of 2,2'-Azobis(2-methylpropionitrile) as thermal initiator. The polymerization was conducted at 75 °C for 8 h, afterwards, the reaction was quenched by

cooling down to room temperature. The crude product was precipitated into an excessive amount of diethyl ether three times followed by room-temperature vacuum drying, yielding the P(HEAA-NHS) polymer powders (yield: ~ 83.5 %). The copolymer was stored under -20°C before use.

4.3. Preparation and characterization of injectable hydrogel adhesive

Injectable PHE-Gel hydrogel adhesives were prepared by mixing the P(HEAA-NHS) (0 %, 5 %, 10 %, and 20 %, w/v) and gelatin (30 %, w/v) evenly using a syringe. The gelation time of the hydrogel adhesive was tested by a DHR rheometer (TA Instruments, New Castle, USA) in a time sweep mode by recording the storage modulus (G') and loss modulus (G'') with the lapse of time after the induction of gelation. The adhesive performance of the hydrogels relative to biological tissues (porcine skin and cartilage) was measured by preparing adhered joints. Interfacial toughness was evaluated by dividing two times of the plateau force by the width of the hydrogel samples. The tensile strength was normalized by dividing the maximal force by the adhesive area.

4.4. Drug-loaded liposome encapsulated hydrogel fabrication and characterization

DMOG-loaded liposomes (DMOG-Lip) were prepared by reverse phase evaporation. In a nutshell, 40 mg of soya phospholipids, 12 mg of cholesterol, and 12 mg of surfactant (DSPE-PEG2000) were dissolved in 5 mL of chloroform solution and added to a round-bottomed flask (Pomex, 5011-100-20). A rotary evaporator at 120 rpm for 3 min was used to remove the organic solvents. After preheating at 50°C , 5 mL of PBS solution containing 35 mg DMOG was added to the flask. Then, a rotary evaporator at 140 rpm for 5 min was used to hydrate. After 5 min of water bath sonication, the liquid was transferred to a centrifuge tube and sonicated on ice for 30 s with an ultrasonic cell disruptor, repeated three times. Then, it was transferred to an ultrafiltration tube (Merck Millipore, UFC910096) and centrifuged at 4°C with $18,000\times g$ for 60 min, repeated three times, adding 1–2 mL of PBS at intervals. Finally, the upper liquid in the ultrafiltration tube was the DMOG-loaded liposomes. The obtained liposomes were stored at 4°C and used up to 1 month after preparation. Transmission electron microscopy (TEM) and Nanoparticle Tracking Analysis (NTA) with a Zetaview (Particle Metrix, Munich, Germany) were performed for the DMOG-loaded liposome size distribution measurement. The DMOG-loaded liposome size was calculated using NTA software (Malvern, Shanghai, China). Dynamic structural changes were identified using Fourier transform infrared spectroscopy (FTIR) on a Nicolet FTIR6700 spectrometer (Thermo Fisher, Massachusetts, USA). The encapsulation rate of the prepared DMOG-Lip was 20.10 % and the drug loading was 10.99 %. Subsequently, the gelatin powder was dissolved in the DMOG-loaded liposomes solution and mixed with P(HEAA-NHS) in the same volume to generate a cohesive hydrogel featuring an even distribution of liposomes. To ensure the consistency of DMOG-Lip concentration for subsequent intervention, the prepared DMOG-Lip solution was diluted by equal volume. Scanning electron microscopy (SEM) was used to characterize the structure of liposomes after loading. The degradation of 10%PHE-Gel@DMOG-Lip was examined with respect to weight loss under 3 mg/mL lysozyme solution at 37°C within one month by using PBS as the control group. At each time point, the samples were removed from solution and weighed. The weight loss ratio was normalized to the initial weight of the samples. Using the dialysis bag method for liposome release experiments in vitro. In short, placed the liposome in the dialysis bag and clamped both ends of the dialysis bag. Then, put the complex into a 50 mL centrifuge tube filled with PBS (pH = 7.4). Transfer the whole system to the shaker and maintain 37°C , 80 r·min⁻¹. Sample 1 mL at the scheduled time (30min, 1h, 2h, 4h, 10h, 12h, 1d, 2d, 4d, 7d) for determining the concentration of released DMOG.

4.5. Cell culturing and maintaining

Mouse embryonic fibroblasts (C3H/10T1/2, C3H10) were purchased from ZQXZBIO (Shanghai, China) and maintained in MEM-alpha with 10 % FBS, 1 % P/S at 37°C under 5 % CO_2 . Subsequent chondrogenic differentiation was performed in the chondrogenic medium containing DMEM, 10%FBS, 110 mg/L sodium pyruvate, 1 % ITS+, 0.15 mM L-Ascorbic Acid 2-Phosphate Sesquimagnesium Salt Hydrate, 40 $\mu\text{g}/\text{mL}$ proline, 10 ng/mL TGF- β 1, 100 nM dexamethasone and 1 % P/S.

Bone marrow-derived macrophages (BMDMs) were isolated from 6- to 8-week-old male C57BL/6J, and the femurs and tibias were collected aseptically in PBS. After exposing the pulp cavity with sterile scissors, RPMI-1640 was used to flush out the bone marrow with a sterile 25-gauge needle. Bone marrow cells were collected with a 70 μm tissue sieve before removing the excess red blood cells with red blood cell lysate (Biosharp). The collected bone marrow cells were cultured in a 10 cm dish overnight at 37°C with 10 % FBS (Pre-inactivated treatment at 56°C for 30min) and 1 % P/S in RPMI-1640. The nonadherent cells were collected via centrifugation and seeded in a 6-well plate at the density of 1×10^6 cells/well. These cells were incubated for 3 days in complete RPMI-1640 supplemented with 10 ng/mL M-CSF. The adherent BMDMs were collected for subsequent experiments. Subsequently added 100 ng/mL LPS for M1 polarization or 20 ng/mL IL4 and 20 ng/mL IL13 for M2 polarization.

4.6. Extracts collection

Previously acquired injectable PHE-Gel hydrogel adhesives were immersed in 10 times the volume of serum-free DMEM. To investigate the effect of the components of the hydrogel on C3H10 cells, incubate the mixture at 37°C for 24 h to allow the hydrogel adhesive to fully release its components into the DMEM. After the incubation period, the resulting solution is the PHE-Gel extract. Without special explanation, all in vitro experiments were performed with extracts.

4.7. Biocompatibility of PHE-gel hydrogel

Cell proliferation was measured by CCK-8 assays according to the manufacturer's protocol with three replicates. C3H10 (4×10^3) was cultured in 96-well plates with 10 % FBS in MEM-alpha overnight. The intervention measures were applied according to the group (con and 10%PHE-Gel) for 1, 2, or 3 days. Then the medium was replaced with 10 μL CCK-8 solution dissolved in 100 μL cell medium. The plate was incubated at 37°C for 1h before absorbance at 450 nm was measured.

The hemolytic assay of the 10%PHE-Gel hydrogel was conducted utilizing fresh rat blood. Fresh blood samples underwent centrifugation at 3000 rpm for 15 min to isolate the red blood cells (RBCs), which were subsequently washed three times with 0.9 % saline solution. The diluted RBCs were then co-cultured with the extracts of the hydrogel at 37°C for 4 h. A positive control, representing 100 % hemolytic efficiency, was established using 0.1 % TritonX-100. The negative control was PBS. Following centrifugation at 3000 rpm for 15 min, the absorbance at 570 nm was quantified using a microplate reader. The hemolysis rate was calculated by comparing the absorbance values of the experimental samples with those of the positive control.

Calcein-AM/PI Cell Viability/Cytotoxicity Assay Kit was used to evaluate cytotoxicity according to the manufacturer's protocol with three replicates. C3H10 (2×10^5) was cultured in 6-well plates with 10 % FBS in DMEM overnight. Then experimental groups were changed to isovolumetric PHE-Gel extracts. After 24 h of intervention, discard the medium and wash with PBS. To prepare the staining solution, Calcein-AM solution, PI solution, and PBS were mixed in a ratio of 1:3:1000, respectively. This mixture was gently vortexed to ensure a homogeneous distribution of the dyes before use in the assay. Added 500 μL of the staining solution and incubated at 37°C for 15min before recording by fluorescence microscopy.

4.8. Cell adhesion

Cytoskeleton staining was used to assess cell adhesion and differentiation. C3H10 was treated with PHE-Gel extracts that were extracted from different adhesive hydrogels for 3 days. The cells were fixed with 4 % PFA before washing with 0.1 % Triton X-100, then incubated with TRITC-Phalloidin and DAPI. The samples were observed using a fluorescence microscope (ECLIPSE Ts2, Nikon).

4.9. Chondral differentiation

C3H10 (2×10^5) was cultured in 6-well plates with 10 % FBS in MEM- α overnight. To determine the optimal hydrogel adhesive properties, experimental groups were changed to isovolumetric PHE-Gel extracts that were extracted from different adhesive hydrogels for 3 days or 7 days. In the follow-up experiment, it was changed to a chondrogenic medium with or without DMOG-Lip containing DMEM or PHE-Gel extracts, chondrogenic medium, and 1 % P/S for 7 days or 14 days. Total RNA from C3H10 was extracted using the nucleic acid purification kit (Omega) according to the manufacturer's instructions. Using 1 μ g of total RNA, reverse transcription (TransScript All-in-One First-Strand cDNA Synthesis SuperMix for qPCR, TransGen) was performed to obtain cDNA, which was subsequently used for the following qRT-PCR experiments. The 2- $\Delta\Delta$ CT method was used to calculate the relative expression of the following genes: chondrogenic genes (Acan, Col2a1, Sox9). The sequences of the target genes were: *glyceraldehyde-3-phosphate dehydrogenase (GAPDH)* forward 5'- TTC CAG GAG CGA GAC CCC ACT A-3' and reverse 5'- GGG CGG AGA TGA TGA CCC TTT T-3'; *ACAN* forward 5'- CAG GCT ATG AGC AGT GTG ATG C-3' and reverse 5'-GCT GCT GTC TTT GTC ACC CAC A-3'; *Col2a1* forward 5'-GGG AAT GTC CTC TGC GAT GAC-3' and reverse 5'- GAA GGG GAT CTC GGG GTT G-3'; *SOX9* forward 5'- GGA AGT CGG TGA AGA ACG GA-3' and reverse 5'- AGA TTG CCC AGA GTG CTC G-3'. Immunofluorescence staining of Sox9 was used to evaluate chondrogenic differentiation. According to standard immunofluorescence procedures, cells that underwent the intervention were fixed with 4 % PFA before washing with 0.1 % Triton X-100, then incubated with monoclonal anti-SOX9 (1:500) overnight, followed by the incubation of Goat anti-rabbit IgG-Alexa Fluor 488 (1:1000), and samples were observed using a fluorescence microscope (ECLIPSE Ts2, Nikon).

Western blot: cells were lysed in RIPA Lysis Buffer containing 1 % Protease inhibitor cocktail and 1 % PMSF for 30 min, followed by centrifugation at 12,000 rpm for 15 min. The supernatant was collected, to which a quarter volume of 5X loading buffer was added and subsequently heated at 100 °C for 15 min. SDS-PAGE polyacrylamide gel electrophoresis was then conducted, and proteins were transferred to a PVDF membrane using the wet transfer method. After sealing each membrane with a solution of 5 % BSA for 1 h, it was incubated overnight with anti-SOX9 (1:1000) and anti-Col II (1:1000) on an orbital shaker at 4 °C. The following day, membranes were incubated with the appropriate HRP-conjugated secondary antibody at room temperature for 1 h. Reactive proteins were detected using enhanced chemiluminescence reagents.

Alcian Blue staining: According to the manufacturer's protocol, the cells were fixed with 4 % PFA, immersed in Alcian acid solution for 3 min, and subsequently incubated with Alcian staining solution for 30 min. Following this, the samples were washed with water for 1 min to obtain a general overview.

4.10. RNA-seq and analysis

Total RNA was extracted using Trizol reagent and its quantity and purity were assessed using a Bioanalyzer 2100. High-quality RNA samples (RIN >7.0) were used for sequencing library construction. mRNA was purified from the total RNA and fragmented. These fragments were reverse-transcribed into cDNA and then used to synthesize U-labeled

double-stranded DNA. After adding adenine bases to the ends, adapters were ligated. The ligated products were amplified via PCR, and the average insert size was 300 ± 50 bp. The final cDNA library was sequenced using the Illumina Novaseq 6000 platform, generating paired-end reads of 2x150 bp. The reads were aligned to the reference genome using HISAT2 and assembled with StringTie. The transcriptomes were merged with gffcompare, and expression levels were estimated using StringTie and Ballgown, calculating Fragments Per Kilobase of transcript and million mapped reads (FPKM) values. Differential gene expression analysis was performed using DESeq2 and edgeR, identifying genes with FDR <0.05 and absolute fold change ≥ 2 as differentially expressed. Further, ClusterGVis v0.1.1 (Jun Zhang, 2023) R package was used to perform mfuzz analysis on all differential genes, and the clusterProfiler v4.11.0.002 (Guangchuang Yu) R package to perform KEGG analysis on the different clustered gene modules obtained from mfuzz analysis.

4.11. Modulation of macrophage polarization

BMDMs (5×10^5) were cultured in 6-well plates with 10 % FBS in DMEM overnight. After LPS-induced M1 polarization for 24h, changed to complete medium or PHE-Gel extracts with or without DMOG-loaded liposomes for 24h. Total RNA from BMDMs was extracted using the nucleic acid purification kit according to the manufacturer's instructions. Using 1 μ g of total RNA, reverse transcription was performed to obtain cDNA, which was subsequently used for the following qRT-PCR experiments. The 2- $\Delta\Delta$ CT method was used to calculate the relative expression of the following genes: M1 polarization genes (iNOS, IL-1 β , TNF- α) and M2 polarization genes (CD206, Arg-1). The sequences of the target genes were: *iNOS* forward 5'- GTT CTC AGC CCA ACA ATA CAA GA-3' and reverse 5'- GTG GAC GGG TCG ATG TCA C-3'; *IL-1 β* forward 5'- CCC AAC TGG TAC ATC AGC ACC TC-3' and reverse 5'- GAC ACG GAT TCC ATG GTG AAG TC-3'; *TNF- α* forward 5'- GGA CTA GCC AGG AGG GAG AA-3' and reverse 5'- CGC GGA TCA TGC TTT CTG TG-3'; *CD206* forward 5'- CTC TGT TCA GCT ATT GGA CGC-3' and reverse 5'- TGG CAC TCC CAA ACA TAA TTT GA-3'; *Arg-1* forward 5'- CTC CAA GCC AAA GTC CTT AGA G-3' and reverse 5'- GGA GCT GTC ATT AGG GAC ATC A-3'.

Immunofluorescence staining of Arg-1 and iNOS was used to analyze the effects of hydrogel and DMOG on the modulation of macrophage polarization. The mature BMDMs were stimulated by LPS for 24h, and the medium was changed to complete medium or PHE-Gel extracts with or without DMOG-Lip for 24h. The BMDMs were fixed with 4 % PFA before washing with 0.1 % Triton X-100, then successively incubated with anti-Arg-1 (1:500) and anti-iNOS (1:500) overnight, followed by the incubation of Goat anti-rabbit IgG-Alexa Fluor 488 (1:1000) and Goat Anti-Mouse IgG-Alexa Fluor 647 (1:200), and samples were observed using a fluorescence microscope (ECLIPSE Ts2, Nikon).

4.12. Animal subcutaneous implantation experiments

After the rabbits were anesthetized with pentobarbital sodium, the hair on both sides of the spine was shaved and routine disinfection was carried out. Following implantation requirements, a 1 cm-long skin incision was made on each side of the spine. Following blunt dissection of subcutaneous tissue, 2 10%PHE-Gel or 10%PHE-Gel@DMOG-Lip implants were placed on each side. The incisions were closed and the subcutaneous tissue and skin were closed with sutures in layers, followed by disinfecting the wounds with iodophor. At 2 weeks, 4 weeks, and 8 weeks after the operation, the skin was cut along the midline of the spine, and the subcutaneous tissue was separated so that the implant material was located on the skin. Gross view and HE staining were used to evaluate the degradation effect of materials. Immunofluorescence staining of Arg-1 and iNOS was used to analyze the modulation of macrophage polarization.

4.13. Rabbit osteochondral autograft transfer system (OATS) surgery

First, rabbits were anesthetized with the general anesthetic sodium pentobarbital. After successful anesthesia, the fur around the bilateral knee joints was shaved. Subsequently, the surgical area of the bilateral knee joints was disinfected with iodine. A curved incision was made on the medial aspect of the knee joint, and the patella was flipped laterally to expose the femoral trochlear groove. A 4 mm diameter trephine was used to create a 5 mm deep hole into the subchondral bone beneath the cartilage, and a cylindrical osteochondral plug was harvested from the trephine. Hydrogel was implanted into the femoral defect, and then the cylindrical osteochondral plug was repositioned within the defect.

Thirty-six New Zealand white rabbits were randomly divided into three groups: Con, 10%PHE-Gel, and 10%PHE-Gel@ DMOG-Lip. Samples were collected at 4 and 8 weeks postoperatively. The gross histological evaluation was scored using the International Cartilage Repair Society (ICRS) and Modified O'Driscoll Score (MODS), where higher scores indicate better repair outcomes [32]. Three independent evaluators, blinded to the experimental conditions, individually scored the samples. Micro-CT was performed to observe subchondral bone repair. All specimens underwent decalcification before histological examination. Immunohistochemical staining of Col I, Col X, and MMP13 was used to assess cartilage degeneration. Safranin O staining was utilized to assess cartilage quality, while Masson's Trichrome Staining was employed to evaluate subchondral bone quality. Immunofluorescence staining of Arg-1 and iNOS was used to analyze the modulation of macrophage polarization.

4.14. Statistics

The analyses were performed using GraphPad Prism software 7.0 (GraphPad Software Inc, USA). An unpaired Student's t-test was employed to evaluate differences between the two groups, while a one-way analysis of variance (ANOVA) with Tukey's post-hoc test was used for comparisons involving more than two groups. Results were presented as mean \pm SD, and significance was defined as $P < 0.05$. All the experiments were performed at least 3 times.

Ethics approval and consent to participate

The experimental design was approved by the Animal Ethics and Experiment Committee of Guangdong Provincial People's Hospital (Reference No. KY-D-2021-402-01).

CRediT authorship contribution statement

Jiaqi Zhou: Writing – original draft, Funding acquisition, Conceptualization. **Xiongfa Ji:** Software, Methodology. **Yu Xue:** Visualization, Methodology. **Wenjie Yang:** Writing – review & editing. **Guoqing Zhong:** Visualization. **Zhiyang Zhou:** Software. **Xingmei Chen:** Formal analysis. **Zehua Lei:** Data curation. **Teliang Lu:** Resources, Data curation. **Yu Zhang:** Resources, Investigation. **Ji Liu:** Writing – review & editing, Supervision. **Limin Ma:** Supervision, Project administration, Funding acquisition, Conceptualization.

Declaration of competing interest

The authors declare that they have no known competing financial interests or personal relationships that could have appeared to influence the work reported in this paper.

Acknowledgements

J.Z., X.J., and Y.X. contributed equally to this work. This work was supported by grants from the National Natural Science Foundation of China (Grant No. 32101097, 32471421, 82472155), the Guangdong

Basic and Applied Basic Research Foundation, China (Grant No. 2022A1515010202, 2023A1515011544, 2023A1515011604, 2023A1515220252).

Appendix A. Supplementary data

Supplementary data to this article can be found online at <https://doi.org/10.1016/j.bioactmat.2025.02.035>.

References

- [1] D.J. Huey, J.C. Hu, K.A. Athanasiou, Unlike bone, cartilage regeneration remains elusive, *Science* 338 (6109) (2012) 917–921.
- [2] D.J. Hunter, L. March, M. Chew, Osteoarthritis in 2020 and beyond: a lancet commission, *Lancet* (London, England) 396 (10264) (2020) 1711–1712.
- [3] W.W. Curl, J. Krome, E.S. Gordon, J. Rushing, B.P. Smith, G.G. Poehling, Cartilage injuries: a review of 31,516 knee arthroscopies, *Arthroscopy* 13 (4) (1997) 456–460.
- [4] J.M. Torpy, C. Lynn, R.M. Golub, JAMA patient page. Knee replacement, *JAMA* 305 (8) (2011) 844.
- [5] N.K. Arden, T.A. Perry, R.R. Bannuru, O. Bruyère, C. Cooper, I.K. Haugen, M. C. Hochberg, T.E. McAlindon, A. Mobasheri, J.Y. Reginster, Non-surgical management of knee osteoarthritis: comparison of ESCO and OARS 2019 guidelines, *Nat. Rev. Rheumatol.* 17 (1) (2021) 59–66.
- [6] J. Klein, Chemistry. Repair or replacement—a joint perspective, *Science* 323 (5910) (2009) 47–48.
- [7] E.E. Vellios, K.J. Jones, R.J. Williams, Osteochondral autograft transfer for focal cartilage lesions of the knee with donor-site back-fill using precut osteochondral allograft plugs and micronized extracellular cartilage augmentation, *Arthrosc Tech* 10 (1) (2021) e181–e192.
- [8] A.J. Guzman, T. Dela Rueda, S.M. Rayos Del Sol, S.A. Bryant, S. Jenkins, B. Gardner, P.J. McGahan, J.L. Chen, Arthroscopic osteochondral autograft transfer system procedure of the lateral femoral condyle with donor-site backfill using osteochondral allograft plug, *Arthrosc Tech* 10 (12) (2021) e2683–e2689.
- [9] S.L. Sherman, E. Thyssen, C.W. Nuelle, Osteochondral autologous transplantation, *Clin. Sports Med.* 36 (3) (2017) 489–500.
- [10] R. Gudas, A. Gudaite, A. Pocius, A. Gudienė, E. Cekanaukas, E. Monastyreckienė, A. Basevicius, Ten-year follow-up of a prospective, randomized clinical study of mosaic osteochondral autologous transplantation versus microfracture for the treatment of osteochondral defects in the knee joint of athletes, *Am. J. Sports Med.* 40 (11) (2012) 2499–2508.
- [11] L. Hangody, G. Vászárhegyi, L.R. Hangody, Z. Sükösd, G. Tibay, L. Bartha, G. Bodó, Autologous osteochondral grafting—technique and long-term results, *Injury* 39 (Suppl 1) (2008) S32–S39.
- [12] L. Hangody, J. Dobos, E. Baló, G. Pánics, L.R. Hangody, I. Berkes, Clinical experiences with autologous osteochondral mosaicplasty in an athletic population: a 17-year prospective multicenter study, *Am. J. Sports Med.* 38 (6) (2010) 1125–1133.
- [13] B. Bao, Q. Zeng, K. Li, J. Wen, Y. Zhang, Y. Zheng, R. Zhou, C. Shi, T. Chen, C. Xiao, B. Chen, T. Wang, K. Yu, Y. Sun, Q. Lin, Y. He, S. Tu, L. Zhu, Rapid fabrication of physically robust hydrogels, *Nat. Mater.* 22 (10) (2023) 1253–1260.
- [14] O. Chaudhuri, J. Cooper-White, P.A. Janmey, D.J. Mooney, V.B. Shenoy, Effects of extracellular matrix viscoelasticity on cellular behaviour, *Nature* 584 (7822) (2020) 535–546.
- [15] P. Agarwal, H.P. Lee, P. Smeriglio, F. Grandi, S. Goodman, O. Chaudhuri, N. Bhutani, A dysfunctional TRPV4-GSK3 β pathway prevents osteoarthritic chondrocytes from sensing changes in extracellular matrix viscoelasticity, *Nat. Biomed. Eng.* 5 (12) (2021) 1472–1484.
- [16] X. Zhao, Multi-scale multi-mechanism design of tough hydrogels: building dissipation into stretchy networks, *Soft Matter* 10 (5) (2014) 672–687.
- [17] Y. Gao, J. Chen, X. Han, Y. Pan, P. Wang, T. Wang, T. Lu, A universal strategy for tough adhesion of wet soft material, *Adv. Funct. Mater.* 30 (36) (2020) 2003207.
- [18] M.B. Guglielmotti, D.G. Olmedo, R.L. Cabrin, Research on implants and osseointegration, *Periodontol* 79 (1) (2000) 178–189.
- [19] H. Liu, X. Hu, W. Li, M. Zhu, J. Tian, L. Li, B. Luo, C. Zhou, L. Lu, A highly-stretchable and adhesive hydrogel for noninvasive joint wound closure driven by hydrogen bonds, *Chem. Eng. J.* 452 (2023) 139368.
- [20] Y. Hua, H. Xia, L. Jia, J. Zhao, D. Zhao, X. Yan, Y. Zhang, S. Tang, G. Zhou, L. Zhu, Q. Lin, Ultrafast, tough, and adhesive hydrogel based on hybrid photocrosslinking for articular cartilage repair in water-filled arthroscopy, *Sci. Adv.* 7 (35) (2021).
- [21] Y. Xiong, X. Zhang, X. Ma, W. Wang, F. Yan, X. Zhao, X. Chu, W. Xu, C. Sun, A review of the properties and applications of bioadhesive hydrogels, *Polym. Chem.* 12 (26) (2021) 3721–3739.
- [22] H.P. Lee, L. Gu, D.J. Mooney, M.E. Levenston, O. Chaudhuri, Mechanical confinement regulates cartilage matrix formation by chondrocytes, *Nat. Mater.* 16 (12) (2017) 1243–1251.
- [23] H. Zhang, L. Wang, J. Cui, S. Wang, Y. Han, H. Shao, C. Wang, Y. Hu, X. Li, Q. Zhou, J. Guo, X. Zhuang, S. Sheng, T. Zhang, D. Zhou, J. Chen, F. Wang, Q. Gao, Y. Jing, X. Chen, J. Su, Maintaining hypoxia environment of subchondral bone alleviates osteoarthritis progression, *Sci. Adv.* 9 (14) (2023) eabo7868.
- [24] J. Fernández-Torres, G.A. Martínez-Nava, M.C. Gutiérrez-Ruiz, L.E. Gómez-Quiroz, M. Gutiérrez, Role of HIF-1 α signaling pathway in osteoarthritis: a systematic review, *Rev Bras Reumatol Engl* (2) (2017) 162–173.

- [25] M. Li, H. Yin, Z. Yan, H. Li, J. Wu, Y. Wang, F. Wei, G. Tian, C. Ning, H. Li, C. Gao, L. Fu, S. Jiang, M. Chen, X. Sui, S. Liu, Z. Chen, Q. Guo, The immune microenvironment in cartilage injury and repair, *Acta Biomater.* 140 (2022) 23–42.
- [26] D.K. Taheem, D.A. Foyt, S. Loaiza, S.A. Ferreira, D. Ilic, H.W. Auner, A. E. Grigoriadis, G. Jell, E. Gentleman, Differential regulation of human bone marrow mesenchymal stromal cell chondrogenesis by hypoxia inducible factor-1 α hydroxylase inhibitors, *Stem Cell.* 36 (9) (2018) 1380–1392.
- [27] M.H. Chen, Y.H. Wang, B.J. Sun, L.M. Yu, Q.Q. Chen, X.X. Han, Y.H. Liu, HIF-1 α activator DMOG inhibits alveolar bone resorption in murine periodontitis by regulating macrophage polarization, *Int. Immunopharmacol.* 99 (2021) 107901.
- [28] X. Ji, H. Shao, X. Li, M.W. Ullah, G. Luo, Z. Xu, L. Ma, X. He, Z. Lei, Q. Li, X. Jiang, G. Yang, Y. Zhang, Injectable immunomodulation-based porous chitosan microspheres/HPCH hydrogel composites as a controlled drug delivery system for osteochondral regeneration, *Biomaterials* 285 (2022) 121530.
- [29] Q. Chen, P. Shou, C. Zheng, M. Jiang, G. Cao, Q. Yang, J. Cao, N. Xie, T. Velletri, X. Zhang, C. Xu, L. Zhang, H. Yang, J. Hou, Y. Wang, Y. Shi, Fate decision of mesenchymal stem cells: adipocytes or osteoblasts? *Cell Death Differ.* 23 (7) (2016) 1128–1139.
- [30] D. Huang, Y. Li, Z. Ma, H. Lin, X. Zhu, Y. Xiao, X. Zhang, Collagen hydrogel viscoelasticity regulates MSC chondrogenesis in a ROCK-dependent manner, *Sci. Adv.* 9 (6) (2023) eade9497.
- [31] H. Yin, Y. Wang, Z. Sun, X. Sun, Y. Xu, P. Li, H. Meng, X. Yu, B. Xiao, T. Fan, Y. Wang, W. Xu, A. Wang, Q. Guo, J. Peng, S. Lu, Induction of mesenchymal stem cell chondrogenic differentiation and functional cartilage microtissue formation for in vivo cartilage regeneration by cartilage extracellular matrix-derived particles, *Acta Biomater.* 33 (2016) 96–109.
- [32] M.P. van den Borne, N.J. Raijmakers, J. Vanlauwe, J. Victor, S.N. de Jong, J. Bellemans, D.B. Saris, International cartilage repair society (ICRS) and oswestry macroscopic cartilage evaluation scores validated for use in autologous chondrocyte implantation (ACI) and microfracture, *Osteoarthr. Cartil.* 15 (12) (2007) 1397–1402.